NAVAL POSTGRADUATE SCHOOL

MONTEREY, CALIFORNIA

THESIS

COMPARISON OF POLARIMETRIC CAMERAS

by

Jarrad A. Smoke

March 2017

Thesis Advisor: R. C. Olsen
Co-Advisor: David Trask

Approved for public release. Distribution is unlimited.

THIS PAGE INTENTIONALLY LEFT BLANK

REPORT DOCUMENTATION PAGE			*Form Approved OMB No. 0704–0188*

1. AGENCY USE ONLY *(Leave blank)*	**2. REPORT DATE** March 2017	**3. REPORT TYPE AND DATES COVERED** Master's thesis

4. TITLE AND SUBTITLE
COMPARISON OF POLARIMETRIC CAMERAS

5. FUNDING NUMBERS

6. AUTHOR(S) Jarrad A. Smoke

7. PERFORMING ORGANIZATION NAME(S) AND ADDRESS(ES)
Naval Postgraduate School
Monterey, CA 93943-5000

8. PERFORMING ORGANIZATION REPORT NUMBER

9. SPONSORING /MONITORING AGENCY NAME(S) AND ADDRESS(ES)
N/A

10. SPONSORING / MONITORING AGENCY REPORT NUMBER

11. SUPPLEMENTARY NOTES The views expressed in this thesis are those of the author and do not reflect the official policy or position of the Department of Defense or the U.S. Government. IRB number ____N/A____.

12a. DISTRIBUTION / AVAILABILITY STATEMENT
Approved for public release. Distribution is unlimited.

12b. DISTRIBUTION CODE

13. ABSTRACT (maximum 200 words)

This thesis is an analysis and comparison of two polarimetric imaging cameras. Previous thesis work utilizing the Salsa Bossa Nova polarimetric camera provided modestly successful results in the application of the camera in determining operational uses of polarization in the field of remote sensing. The goal of this thesis is to compare polarimetric data between two cameras designs and analyze the capabilities of a newly obtained polarimetric camera from Fluxdata. The Fluxdata and Salsa cameras utilize two different techniques to capture polarized light. The Salsa uses a Division of Time Polarimeter (DoTP), which is sensitive to movement, and the Fluxdata camera uses a Division of Amplitude Polarimeter (DoAmP), which is designed to split the incoming light without errors from scene movement. The assumption is that the new Fluxdata camera will be able to capture higher-quality polarization data that can be used in classifying objects in moving scenes. The results of the study confirmed both cameras' display correct polarization signatures and the movement of objects is not affected by the Fluxdata. The Fluxdata displays more detailed polarization signatures, but still suffers from registration errors that are inherent to the focal plane alignment of the DoAmP design.

14. SUBJECT TERMS polarimetric imaging, polarization, polarimetric camera, remote sensing, space systems	**15. NUMBER OF PAGES** 93
	16. PRICE CODE

17. SECURITY CLASSIFICATION OF REPORT	**18. SECURITY CLASSIFICATION OF THIS PAGE**	**19. SECURITY CLASSIFICATION OF ABSTRACT**	**20. LIMITATION OF ABSTRACT**
Unclassified	Unclassified	Unclassified	UU

NSN 7540–01-280-5500

Standard Form 298 (Rev. 2–89)
Prescribed by ANSI Std. 239–18

THIS PAGE INTENTIONALLY LEFT BLANK

Approved for public release. Distribution is unlimited.

COMPARISON OF POLARIMETRIC CAMERAS

Jarrad A. Smoke
Lieutenant, United States Navy
B.S., United States Naval Academy, 2010

Submitted in partial fulfillment of the
requirements for the degree of

MASTER OF SCIENCE IN SPACE SYSTEMS OPERATIONS

from the

NAVAL POSTGRADUATE SCHOOL
March 2017

Approved by: R. C. Olsen
Thesis Advisor

David Trask
Co-Advisor

James Newman
Chair, Space Systems Academic Group

THIS PAGE INTENTIONALLY LEFT BLANK

ABSTRACT

This thesis is an analysis and comparison of two polarimetric imaging cameras. Previous thesis work utilizing the Salsa Bossa Nova polarimetric camera provided modestly successful results in the application of the camera in determining operational uses of polarization in the field of remote sensing. The goal of this thesis is to compare polarimetric data between two cameras designs and analyze the capabilities of a newly obtained polarimetric camera from Fluxdata. The Fluxdata and Salsa cameras utilize two different techniques to capture polarized light. The Salsa uses a Division of Time Polarimeter (DoTP), which is sensitive to movement, and the Fluxdata camera uses a Division of Amplitude Polarimeter (DoAmP), which is designed to split the incoming light without errors from scene movement. The assumption is that the new Fluxdata camera will be able to capture higher-quality polarization data that can be used in classifying objects in moving scenes. The results of the study confirmed both cameras' display correct polarization signatures and the movement of objects is not affected by the Fluxdata. The Fluxdata displays more detailed polarization signatures, but still suffers from registration errors that are inherent to the focal plane alignment of the DoAmP design.

THIS PAGE INTENTIONALLY LEFT BLANK

TABLE OF CONTENTS

THIS PAGE INTENTIONALLY LEFT BLANK

LIST OF FIGURES

THIS PAGE INTENTIONALLY LEFT BLANK

LIST OF ACRONYMS AND ABBREVIATIONS

3D	Three Dimensional
CCD	Charge Coupled Device
DoAmP	Division of Amplitude Polarimeter
DoLP	Degree of Linear Polarization
DoP	Degree of Polarization
DoTP	Division of Time Polarimeter
EM	Electromagnetic
ENVI	ENvironment for Visualizing Images
IDL	Interactive Data Language
IP	Internet Protocol
LCD	Liquid Crystal Display
nm	nanometer
NPS	Naval Postgraduate School
PST	Pacific Standard Time
RAM	Random Access Memory
ROI	Region of Interest
SAR	Synthetic Aperture Radar
USB	Universal Serial Bus

THIS PAGE INTENTIONALLY LEFT BLANK

ACKNOWLEDGMENTS

I give many thanks to Professor Olsen, the staff of the Remote Sensing Center, and my family for all their support. Specifically, a very special thank you to Jeremy Metcalf, who dedicated his time and knowledge to make this possible.

THIS PAGE INTENTIONALLY LEFT BLANK

I. INTRODUCTION

Polarization is one of the four characteristics of light viewed in remote sensing Wavelength/frequency (color), amplitude (intensity), and coherence (lasers) are the other characteristics of light that are used when imaging scenes. Polarimetric imaging is a relatively new field in the remote sensing community. The advantages of polarimetric imaging to detect and categorize objects is not a high priority topic in the realm of remote sensing. The use of polarization in remote sensing and its interaction with the world is yet to be clearly portrayed as a major advantage over traditional panchromatic and multispectral imaging. This research compares and verifies polarization signatures from previous work with a polarization camera. The image comparison addresses the effects of polarization in remote sensing and potential uses.

The primary objective is to determine the similarities and differences of the images captured and compare how each camera captures and depicts the effects of polarization. Additionally, the advantages and disadvantages of the specific techniques and capabilities of the cameras are analyzed to further understandings of how imaging can be utilized to find a common ground for polarization imaging. The use of these polarization cameras help the human eye distinguish features of both natural and man-made objects that are normally ignored in traditional remote sensing techniques. A brief overview and history of polarization are presented to better understand the analysis of the images collected using the two polarization cameras.

A. POLARIZATION EXPLAINED

Humans view the intensity of light as the various colors of the spectrum. Characteristics of light include amplitude (intensity), frequency (color), polarization, and coherence (Schott 1998, 4). The value of use follows the nature and use of color used by humans. The human eye has cone cells, displayed in Figure 1, that correspond reflected light from objects into colors which range from wavelengths of approximately 400–700nm (Olsen 2015, 61). It is difficult for the human eye to interpret polarized light, but some insects can view polarized and ultraviolet light (Temple 2015). Insects have special

photoreceptors that distinguish the electric field orientation which characterizes the polarization effect used by bees and ants to navigate.

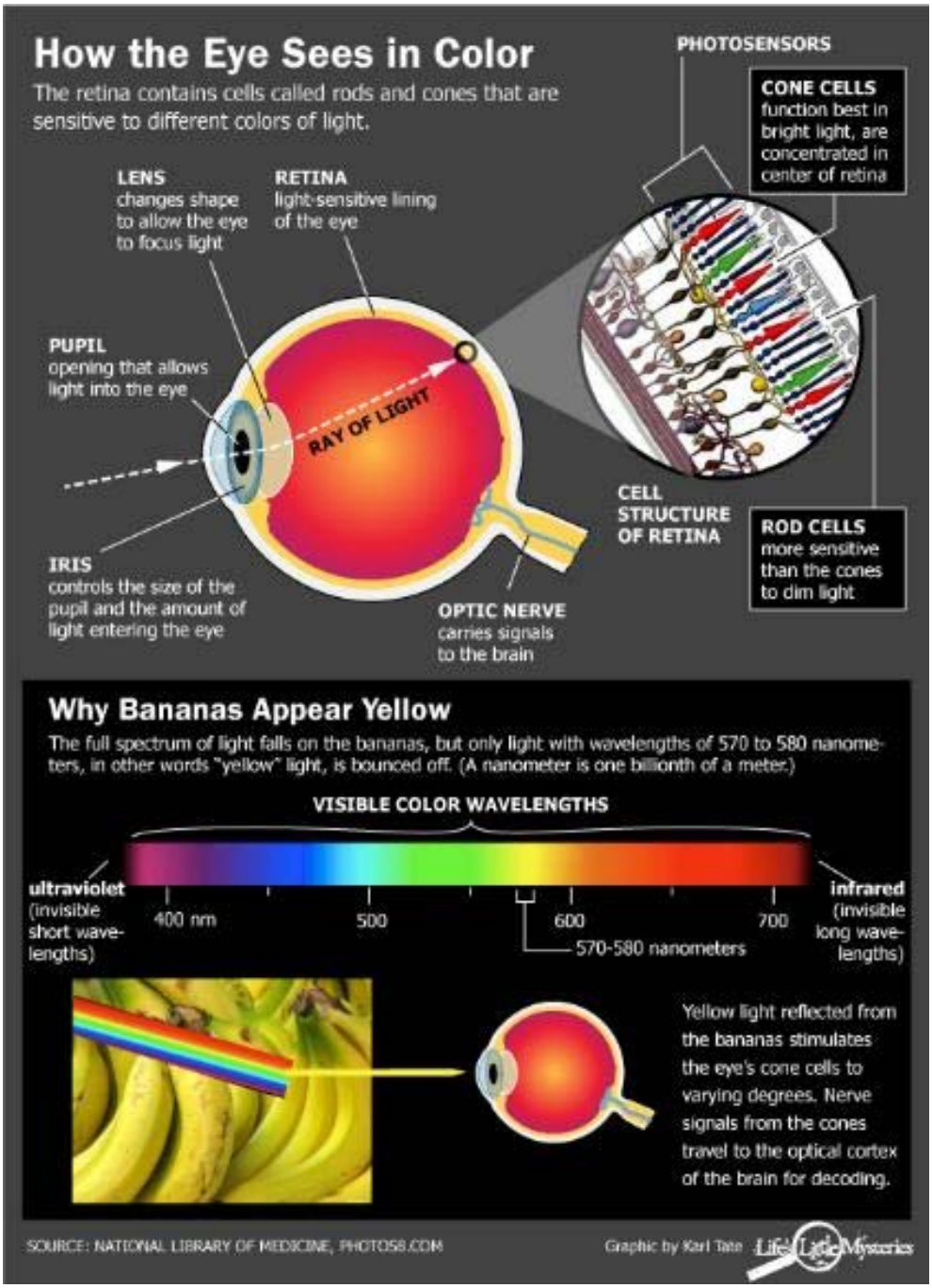

Figure 1. Human Eye Viewing Light. Source: Pappas (2010).

The naked eye can be trained to distinguish polarized from nonpolarized light with the concept of Haidinger's brushes (Temple 2015). Polarized light occurs when a light waves' electric field is on distinct plane perpendicular to the transverse waves, as seen in Figure 2. Naturally occurring light can be unpolarized, partially polarized, or fully polarized. Sources of light include the sun, lightbulbs, candles, or any light creating object. Once light encounters a surface, it becomes partially polarized, fully polarized, or remains unpolarized, depending on the surface, material, roughness, and incidence angle. The production of polarized light is caused by absorption, refraction, reflection, diffraction, and birefringence. To understand polarization, a basic understanding of the characteristics of electromagnetic radiation through Maxwell's equation is needed.

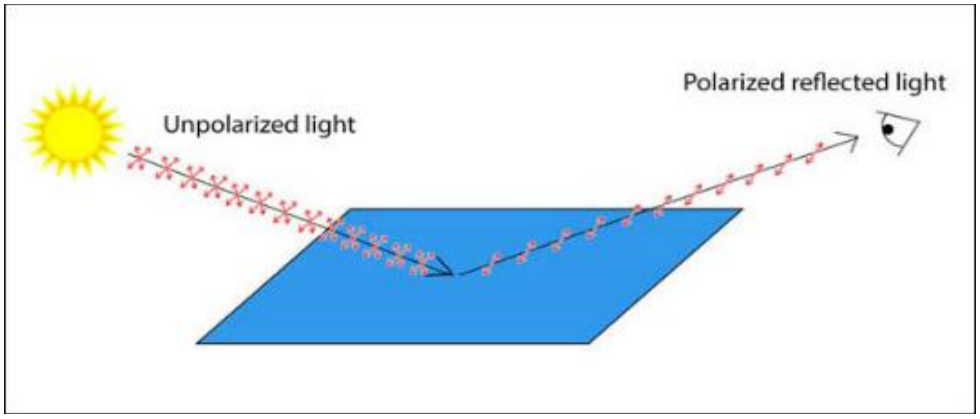

Figure 2. Viewing Polarization after Being Reflected from Horizontal Surface. Source: Collett (2005).

Maxwell's equations explain electromagnetic radiation and describe polarization for a transverse wave; displayed mathematically and represented in three-axis graph in Figure 3. The direction of the electric field is how polarization is determined. If the electric field is well defined in a certain direction, then the light is polarized. The light is unpolarized if the electric field is randomly oriented without a distinct direction.

$$\nabla \times \mathbf{H} = \mathbf{J} + \frac{\partial \mathbf{D}}{\partial t}$$

$$\nabla \times \mathbf{E} = -\frac{\partial \mathbf{B}}{\partial t}$$

$$\nabla \cdot \mathbf{D} = \rho$$

$$\nabla \cdot \mathbf{B} = 0$$

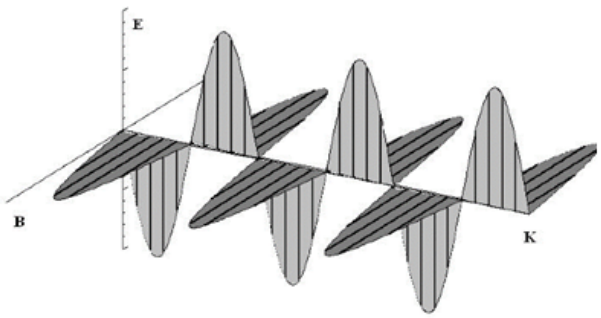

E Is The Electric Field, B Is The Magnetic Induction Field, D Is The Electric Displacement, H Is The Magnetic Field, J Is Electric Current, T Is Time.

Figure 3. Maxwell's Equations. Source: Olsen (2015).

The simplest way to view a plane of polarization is by removing all unwanted polarization orientations. Viewing an image that allows only vertical polarization will eliminate the light in the horizontal field and all other angles of polarization besides the vertical state. This aspect of polarization may help improve the appearance of vegetation, eliminate glare from roads, view into bodies of water, or determine objects with polarized material.

The primary and most common way to measure and view polarization is through Stokes parameters. Stokes vector representation of a polarized beam represent both fully and partially polarized beams (Schott 2009, 33). An advantage of Stokes vectors is that there is no preferred orientation when associating them with the electric field (Schott 2009, 33). Stokes parameters are observable quantities displayed in terms of optical intensities as shown in Figure 4 (Schott 2009, 34). The terms S0, S1, S2, and S3 are synonymously referred to as I, Q, U, and V, respectively. The S0 term is the total energy of a beam or intensity of light captured, effectively the unpolarized light (Olsen 2015, 140). The S0 term is also how a typical panchromatic image would be represented. The next two terms describe linear polarization. S1 is the difference between light polarized at 0 and 90 degrees. S2 is the difference between polarized light at +45 and -45 degrees. S3 describes the difference of right and left hand circular polarization. Circular polarization in the S3 term is generally ignored in viewing polarization because it is rarely found in nature (Olsen 2015, 140).

$$S_0 = I_{0°} + I_{90°}$$
$$S_1 = I_{0°} - I_{90°}$$
$$S_2 = I_{45°} - I_{-45°}$$
$$S_3 = I_{rh} - I_{lh}$$

Polarization State	Symbol	Stokes Vector
Horizontal	↔ ⊥ S	$\begin{pmatrix}1\\1\\0\\0\end{pmatrix}$
Linear +45 deg	⤢	$\begin{pmatrix}1\\0\\1\\0\end{pmatrix}$
Right-Hand Circular	↻	$\begin{pmatrix}1\\0\\0\\1\end{pmatrix}$
Random	*	$\begin{pmatrix}1\\0\\0\\0\end{pmatrix}$

Polarization State	Symbol	Stokes Vector
Vertical	↕ ‖ P	$\begin{pmatrix}1\\-1\\0\\0\end{pmatrix}$
Linear −45 deg	⤡	$\begin{pmatrix}1\\0\\-1\\0\end{pmatrix}$
Left-Hand Circular	↺	$\begin{pmatrix}1\\0\\0\\-1\end{pmatrix}$

Figure 4. Stokes Vectors. Source: Schott (2009).

Various products can be calculated from the acquired Stokes vectors to display polarization images and video. Some of these calculations include degree of polarization, angle of polarization, inverse intensity, and color mapping techniques. Each of these calculations mathematically calculate each pixel to determine the output product.

The degree of linear polarization (DoLP) or degree of polarization (DoP) is the percentage of linear polarization in the electromagnetic wave. We calculate DoLP using Stokes vectors as seen in Figure 5. Each pixel value is calculated and varies from 0 (unpolarized) to 1 (polarized), with values in between being partially polarized.

$$\mathrm{DoP} = \frac{\sqrt{S_1^{\,2} + S_2^{\,2}}}{\mathrm{S}_0}$$

Figure 5. Degree of Linear Polarization (DoLP) or Degree of Polarization (DoP) Equations Source: Schott (2009).

The resulting image represents the fraction of polarization for each pixel. The representation helps distinguish polarized objects. The DoLP is typically represented with black as 0% linear polarization and white as 100% linear polarization, with values in between as a grayscale.

Color combination of Stokes vectors are used to associate Stokes parameters to a color such as Red for S0, Green for S1, and Blue for S2 to distinguish objects with stronger polarizations in each field. An alternative approach developed by Tyo displayed an HSV (Hue, Saturation, Value) representation in which the hue is the angle in color space (ranging from 0–360), saturation (ranging from 0 (neutral gray) to 1 (pure color), and value is the brightness of the scene, spanning from 0 to maximum brightness as displayed in Figure 6 (Tyo 1998).

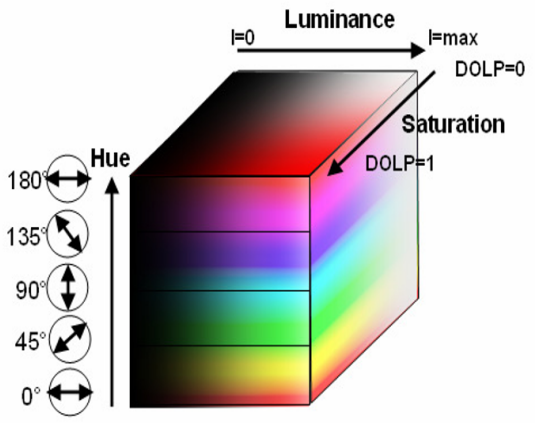

Figure 6. HSV Representation. Source: Smith (2008).

B. OPTICAL POLARIZATION

Optical polarization involves the use of filters to capture light and view scenes in a different perspective. Filters, also known as polarizers, differentially transmit or reflect electromagnetic radiation based on the orientation of the electric field to distinguish polarization. The perfect filter absorbs all of a distinct state of polarization and transmits all other orientations of polarization as shown in Figure 7. Polarimetric imaging is used in remote sensing, microscopy, stress testing, and various other sensing fields to discover new characteristics that are not seen through traditional viewing techniques.

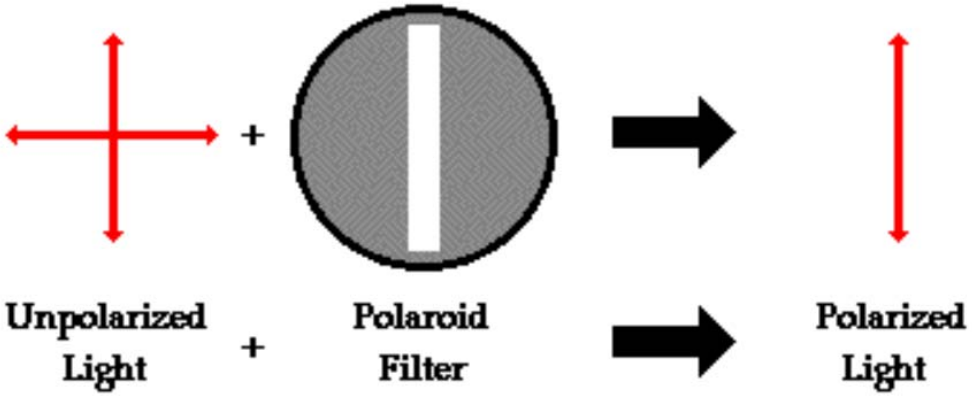

Figure 7. Polarized Filter. Source: Henderson (2017).

Filters include linear and circular types made of wire grid polarizers, dichroic and birefringent polarizers. Wire grid polarizers and sheet polarizers consist of very thin layers of metallic materials aligned with each other to transmit a specific direction of the electric field, while absorbing or reflecting the perpendicular field, as shown in Figure 8. Similar effects are found in nature in crystals. A dichroic polarizer absorbs a certain polarization of light and transmit the rest, while a birefringent polarizer is dependent on the refractive angle that it absorbs. Including these materials on cameras and detectors aid in the measurement of the polarization state of a beam.

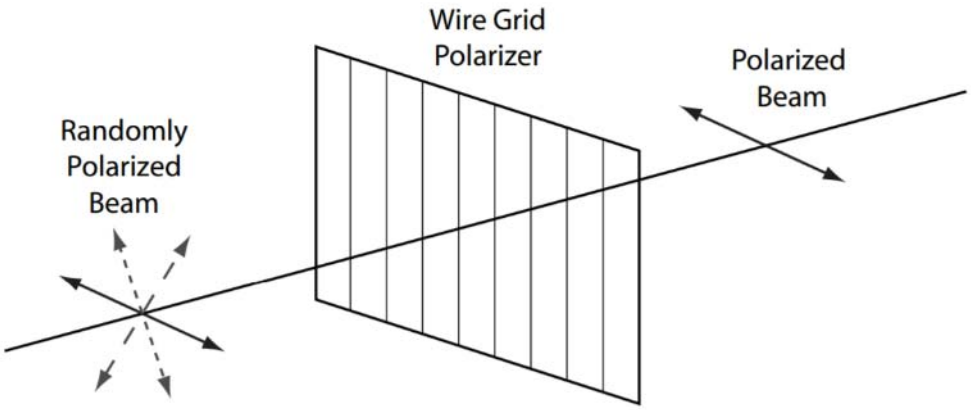

Figure 8. Wire Grid Polarizer. Source: Schott (2009).

Polarimetric interactions in remote sensing describe the behaviors of the polarized beam with a reflective or transmissive medium (Schott 2009, 51). Light interacts with surfaces through transmission, reflection, scattering, or absorption as shown in Figure 9. These interactions are based on the physical properties of the object, the wavelength of the incident radiation, and the angle at which the wave hits the surface (Olsen 2015, 45).

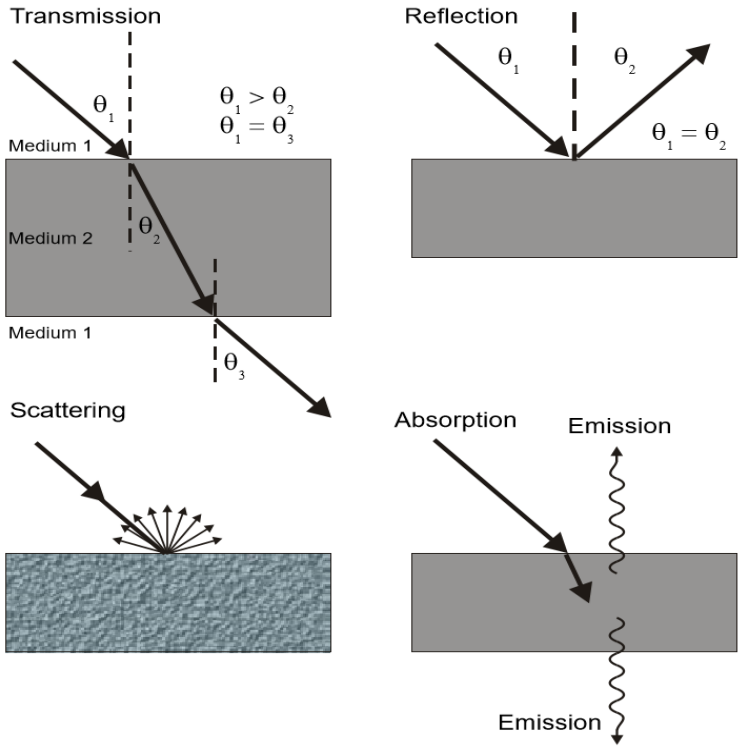

Figure 9. Light Interactions. Source: Olsen (2015).

Polarization by reflection occurs when unpolarized light interacts with a surface and the reflected light undergoes a polarization change. Fresnel's equation and depictions in Figure 10 explains how the polarization state change is affected by the angle of incidence, where r is the ratio of the amplitude of the reflected electric field to the incident field and n1, θ1 and n2, θ2 are the refractive indices and angles of incidence and refraction (Olsen 2015, 46). Similarly, the transmittance of polarized waves interacts when they pass through matter without a measurable change in attenuation (Olsen 2015, 45).

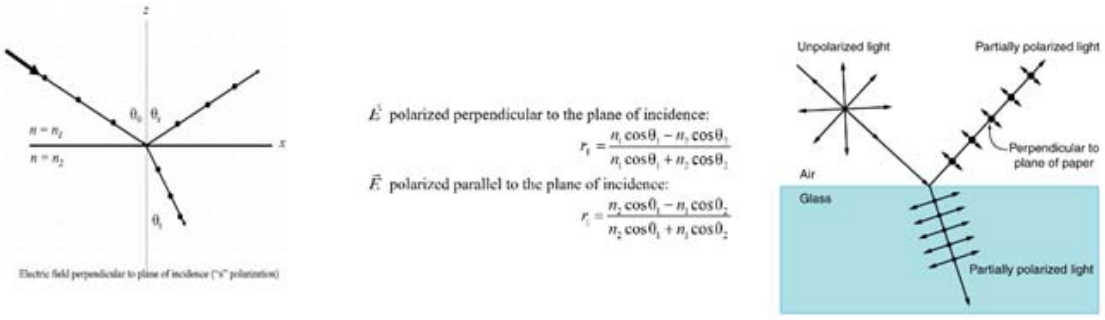

Figure 10. Transmittance and Reflectance for Polarized Light.
Source: Easton (2004).

Polarization by scattering is like reflection but the resulting polarization is dispersed in an unpredictable direction. Rayleigh scattering, depicted in Figure 11, occurs when particles are much smaller than the incident wavelength.

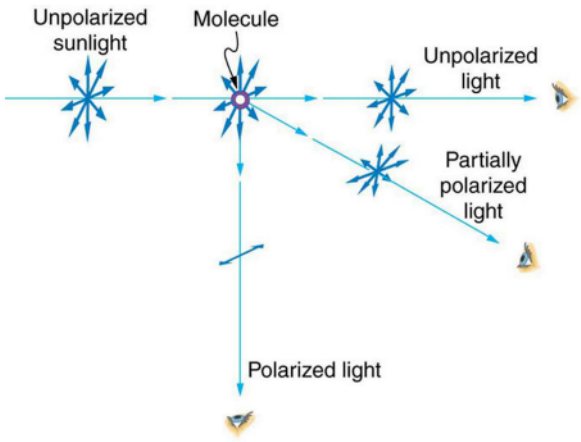

Figure 11. Polarization by Scattering. Source: Boundless (2016).

Polarization absorption occurs when the incoming radiation is taken in by a medium and not transmitted (Olsen 2015, 47). Certain crystals and Polaroid film uses the process of absorption of polarized states to absorb distinct polarization states.

The UMOV effect is the phenomenon in which the degree of linear polarization is inversely proportional to a material's reflectance or albedo (Schott 2009, 73). Interparticle scattering causes an increased albedo and decreased polarization (Zubko

2011). An object with a bright surface will tend to have a lower degree of polarization and darker objects will have higher degrees of polarization. Quantitative data has been collected on the moon that displays the UMOV effect for different phases and regions of the moon (Zubko 2011). The effect relates the wavelength, color, and texture of an object to polarization.

C. NON-OPTICAL POLARIZATION

Communications and radar applications also utilize polarization to control electromagnetic radiation to propagate signals. Both linear and circular polarization waves are used to transfer information and receive electromagnetic radiation. Polarized filters work similarly in the non-optical field with the type of antenna chosen when sending and receiving data. Antennae have the capability to transmit and receive various horizontal, vertical, and circular radiation formats. One example is a right hand circular antenna may only accept other right hand circular signals, thus eliminating other signals being transmitted. Radar antennae work in a similar fashion to transmit signals and receive the requested polarization signal to determine objects and images. A design of dual polarization radar sends both vertical and horizontal electromagnetic waves and computes cross sectional areas to classify size and shapes of objects with improvements in rainfall estimation, precipitation classification, data quality and weather hazard detection (NOAA).

D. MODERN APPLICATIONS OF POLARIZATION

The most common use of polarization in everyday use are polarized sunglasses. This technology eliminates glare from vectors of polarization that are reflected from roads or water. Most glare comes from horizontal surfaces such as highways and water. A pair of sunglasses designed to eliminate glare might be vertically polarized to eliminate the horizontal glare and only allow vertically polarized light through the glasses.

Some light sources are polarized such as lasers and monitors. Certain television or computer monitors have polarized films or layers to control the intensity of light viewed by the user. Liquid Crystal Displays (LCD) use polarization to control different intensities of colors. Not all lasers are polarized, but some devices such as interferometers,

semiconductor optical amplifiers, and optical modulators use polarized lasers to achieve their desired results.

Displaying 3D movies and images is possible because of polarization. 3D imaging uses two images overlaid on the same screen with the use special polarized glasses creating a 3D image. With a different polarized filter on each lens, the human eye sees two images that create the 3D image.

The use of polarization in microscopic science has led to the discovery of how different anisotropic substances interact with polarized light. Anisotropic substances interact differently under polarized light and do not behave the same way in all directions. Polarization microscopes are used in medical fields and geological research. The basic concept and design of a polarizing microscope is displayed in Figure 12.

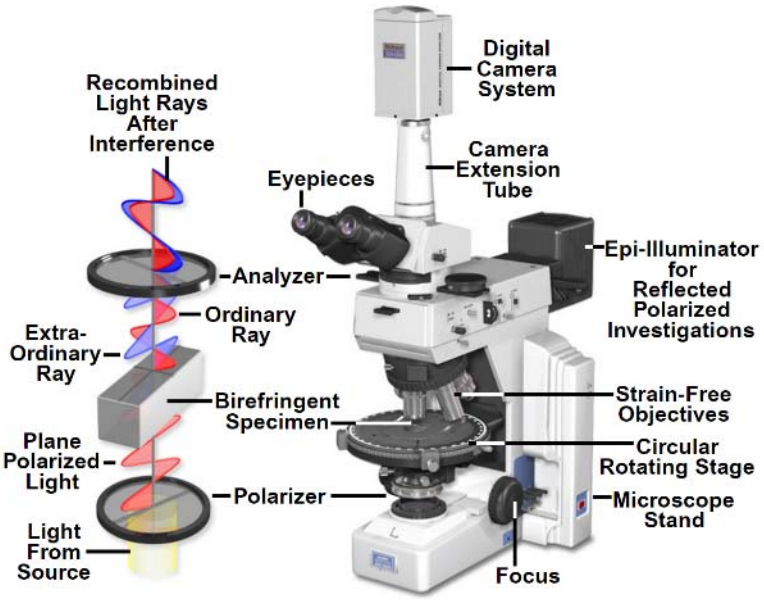

Figure 12. Polarizing Microscope. Source: Robinson (2016).

Satellites and radar utilize polarization in the optical and non-optical fields. Communication and radar imagery use polarization to transfer information in military and commercial products. Synthetic Aperture Radar (SAR) onboard TerraSAR-X and

airborne assets such as AIRSAR utilize different polarization signatures when imaging (Lou). Figure 13 displays a product of polarized radar imagery.

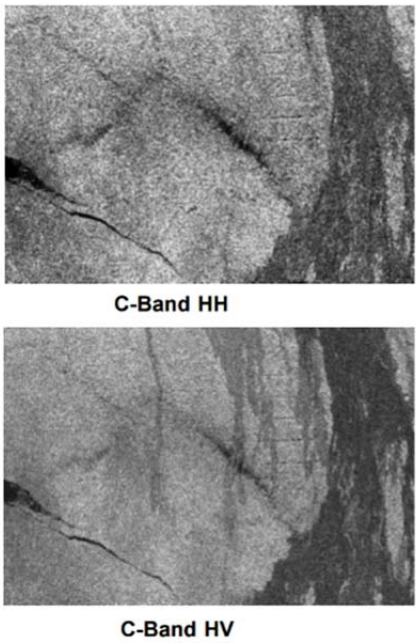

Figure 13. Polarized RADAR Imagery. Source: Smith (2012).

II. HISTORY

The origins of polarization date back to the 11th century with experiments verifying the ray theory of light and the law of reflection (Collett 2005, 1). Polarization observations began in scientific studies in the late 19th century with early understandings dating back to 1669 (Brosseau 1998, 1). Through folklore, the possibility of Vikings using polarization of the sky light to navigate dates to 700 (Brosseau 1998, 3). The history of polarization studies can be broken down into three distinct research periods that lead us to the modern study of polarization based on ideas and observations from Bartholinus to Stokes, the electromagnetic nature of light, and the coherence and quantum properties of light.

A. FIRST PERIOD: 1669–1864

In the seventeenth century, the study of polarization started with the optical observations of light and geometric measurements showing that it as an instantaneous propagation of an action through a medium (Brosseau 1998, 3). Erasmus Bartholinus is typically given credit in discovering polarization in 1669 with the demonstration of double refraction using a crystal made of calcite (Brosseau 1998, 3). Depicted in Figure 14, Bartholinus showed how a single ray of light consisted of two separate rays when propagated through a rhombohedral calcite crystal. Shortly after, Dutch physicist, Christiaan Huyghens, added a second calcite crystal and determined that the two beams passing through a second crystal could be manipulated to maximize and minimize the intensity of light, demonstrating different polarization directions (Brosseau 1998, 4). Huyghens developed the geometric theory to determine all optical occurrences including reflection, refraction, and double refraction (Brosseau 1998, 4). Following these discoveries, Newton's particle theory of light verified light as a beam comprised of rays identified by geometric lines consisting of streams of particles (Brosseau 1998, 4). Following these discoveries, Newton's great standing and views on light led to a slow development of polarization until the establishment of the wave theory of light in the nineteenth century.

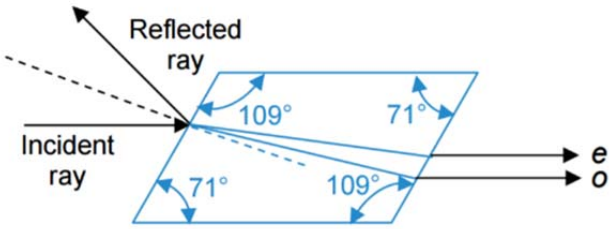

Figure 14. Double Refraction Source: Collett (2005).

In 1803, Thomas Young displayed the effect of polarization from the transverse nature of light, which countered Newton's concepts on destructive interference of light (Brosseau 1998, 4). Etienne-Louis Malus discovered the polarization of natural light by reflection. He experimented and geometrically reasoned how to explain the intensities of light from a polarizing crystal. His work shows how to filter out polarized light and Figure 15 displays the effects of a how natural incident light becomes polarized when reflected by glass. He showed how the light reflected could be extinguished at an approximate angle of incidence of 57 degrees.

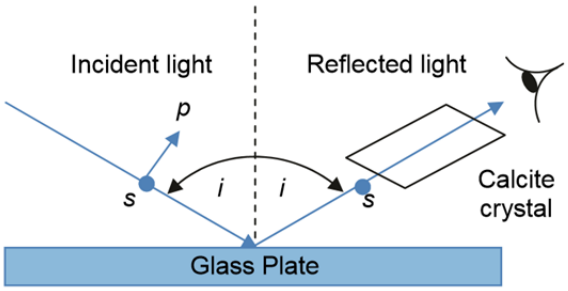

Figure 15. Malus' Glass Plate. Source: Collett (2005).

Expanding on Malus's glass plate experiment, Sir David Brewster discovered the relation between the refracted ray and incidence angle when observing light through a crystal reflected off a glass surface, shown in Figure 16. He determined that there is a particular angle of incidence that extinguishes light and that complete polarization occurs when the angle of incidence equals this angle (Brewster's angle) (Brosseau 1998, 5). The Brewster angle determined the neutral point of polarization in the sky.

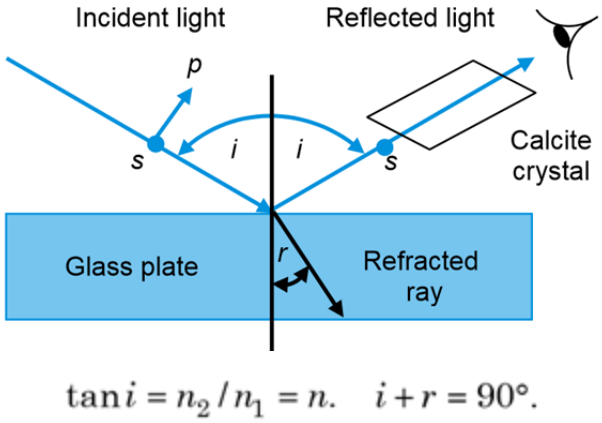

Figure 16. Brewster's Law. Source: Collett (2005).

Augustin Jean Fresnel furthered the understanding of the modern view of polarized light and the wave theory of light with his work on reflection and transmission formulas which recognized the phenomenon of certain material to have an index of refraction for right and left circular polarized light (Brosseau 1998, 5). Along with François Arago, Fresnel contributed to the laws of interference of polarized light. Additionally, the creation of the optical microscope and polariscope in the nineteenth century advanced studies in the polarization signature details of minerals and various materials (Brosseau 1998, 6).

Sir Georges Stokes introduced the Stokes parameters, which were measurable quantities of the properties of polarized light; depicted in Figure 17. The Stokes' parameters mathematically describe the state of polarization, to include partially and polarized light (Brosseau 1998, 7). His explanation of the polarized light was based on intensities at optical frequencies, with the first parameter signifying total intensity and the remaining three describing the state of polarization for linearly, diagonal, and circular polarization.

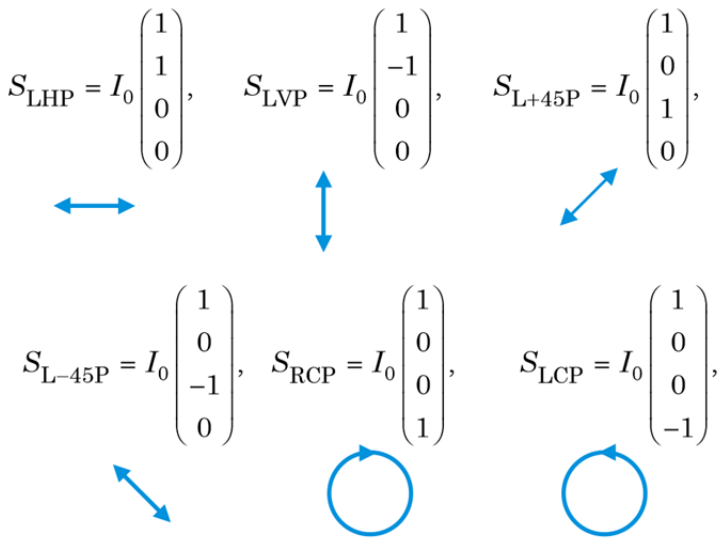

Figure 17. Stokes Vectors. Source: Schott (2009).

Giorgo Govi's experimentations on light concluded that small particles scattering light is not reliant on the reflection of light, leading to research of the scattering of radiation by matter. Govi's research helped pave the path for John Tyndall to demonstrate the scattering of light by particles was dependent on particle size and how very fine particles perfectly polarize light at a 90 degree angle (Brosseau 1998, 8). Tyndall's research in 1869 led to inventions to conduct research about the color of the sky and water.

B. SECOND PERIOD 1864–1920

Maxwell's theory of the electromagnetic (EM) nature of light established a new era of observation and research in the polarimetry field of science. Maxwell's differential equations based on Faraday's concepts put EM waves into transverse wave solutions. His theory of the EM characteristics of light led to new research of unpolarized and polarized light with application of polarizers, electric fields, and magnetic fields by scientists including John Kerr, Emile Verdet, and many others (Brosseau 1998, 11). An example is Pieter Zeeman's experiments and how he predicted the nature of polarization based on EM fields, further verifying the acceptance of the EM theory of light (Brosseau 1998,

12). These discoveries also involved research in other fields including radio and microwave communications.

Lord Rayleigh's contribution to polarization includes his theory of polarization at 90 degree angles and the intensity of light scattered by particles. Rayleigh's law of polarization at 90 degrees describes scattered light's highly linearly polarized properties in the sky. His law on intensity of light explained the correlation of the dependence of the degree of polarization from scattered light on the angle of its scattering. Additionally, Nikolay Umov, conveyed the relationships between polarization and surface roughness (Brosseau 1998, 13). These theories led to major advancements in understanding the scattering of EM waves by a sphere.

C. THIRD PERIOD: 1920–PRESENT

The final phase of research in polarization's process of emission and absorption by matter was best explained by the end of the nineteenth century with the development of the quantum theory in the twentieth century. Maxwell's theory explained the observable features of light and the quantum theory led to the acceptance of photons. The quantum treatment of polarization was studied and researched to relate back to the classical understanding of polarized light based on the theory of the coherence of light.

The invention of the modern sheet polarizer was developed in 1927 by orientating crystalline needles of herapathite in a sheet of plastic. This invention focused attention on describing changes in the state of polarized light and how it undergoes change while interacting with optical elements. 1928 marked the first use of polarization in remote sensing of planetary surfaces by French astronomer Bernard Lyot (Brosseau 1998, 19). Lyot invented optical devices including the double-refraction filter and a depolarizer consisting of two retardation plates, with a retardation ratio of 1:2 and their axes oriented at 45 degree to another (Brosseau 1998, 19). Depolarizers are used to transform polarized light into unpolarized light, which is essential in modern day fiber optics devices.

The term ellipsomtery describes the effect insects utilize to orient themselves with their eyes by using the polarization of sky light (Brosseau 1998, 19). This led to the discovery of the human eye being able to detect and distinguish the difference of left and

right hand circular polarized light, with the understanding that the human eye is not capable of distinguishing linear polarization. Much advancement in communication theory was developed around World War II, including mathematical and statistical properties of polarization that helped develop radar that could detect aircraft.

The brief history of polarization gives a great insight on how the theories and experiments developed into today's modern uses of polarization. Reviewing the progress made through these three major periods, we can implement old and new ideas into the study of polarization for remote sensing today. These concepts will be applied in the analysis of the images captured with polarimetric cameras and help verify polarization states and signatures.

III. CAMERA OPERATIONS

A. SALSA

The Bossa Nova Tech Salsa polarization camera offers both polarization analysis and regular digital video camera capabilities. The plug-and-play use of the Salsa makes it easy to setup and take images. The ability to display full Stokes parameters and calculations in real time on each pixel is the main feature in the Salsa camera. The Salsa camera, displayed in Figure 18, comes with specialized software that provides real time calculations and is easy to use view and output data.

Figure 18. Salsa Camera. Source: Salsa.

The Salsa camera technology uses a patented polarization filter based on a ferroelectric liquid crystal which reduce the acquisition time when taking images. The Salsa's fast switching liquid crystal polarizing filter separates polarized light onto a 782 x 582 pixel detector operating in the 400 to 700 nm range (West). The camera has a standard 12-bit CCD lens, one megapixel, and F mounted lens that is interchangeable. The Salsa has an ARSAT H 20mm with an F number of 2.8 and uses a Hoya 52mm green filter which allows the LCD polarizer to operate within the specified spectral bandwidth from 520–550 nm. The camera is powered by a fifteen-volt direct current and has a

FireWire and USB connection for data input/output to a connected computer. The camera's parts are mounted in a small rectangular box (4" × 4" × 6"), as depicted in Figure 19.

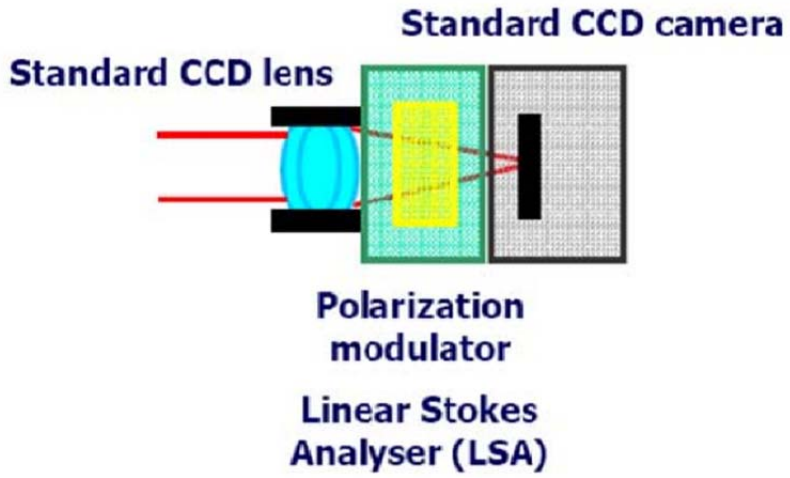

Figure 19. Salsa Camera Mechanism. Source: Salsa.

The Salsa uses a division of time polarimeter (DoTP) to capture imagery. It uses sequential images taken with the polarization filter rotated to different orientations to construct the linear Stokes vectors. The software then calculates the Stokes vectors pixel by pixel using a modified Pickering method shown in Figure 20. The limitation in the Salsa is that movement in the target or camera results in a miscalculation between each pixel in the rotating frames. This restriction limits the Salsa's use to laboratory and static scenes.

$$S_0 = \frac{\Phi_0 + \Phi_{45} + \Phi_{90} + \Phi_{-45}}{2}$$

$$S_1 = \Phi_0 - \Phi_{90}$$

$$\mathrm{S}_2 = \Phi_{45} - \Phi_{-45}.$$

Figure 20. Modified Pickering Method. Source: Schott (2009).

The software provided with the Salsa camera was utilized on a MacBook Pro Boot Camp running Windows XP. The Boot Camp image has an Intel Core 2 CPU, 2.33 GHz processor and 2GB of RAM. The Salsa measures intensity and cycles through polarization angles of approximately 0, 45, 90, and 135, shown in Figure 22. These angles correspond to the frames the Salsa calculates the Stokes vectors, but are not exact angle measurement, rather the camera is designed to perform image modulation at orthogonal angles to each other. The camera's software calculates Stokes vectors and various other representations to include DoLP, angle as a color hue, angle, virtual polarization and various other representations of polarization as shown in Figure 21. Each pixel is calculated to provide precise polarization results. Registering images is not required for the Salsa camera.

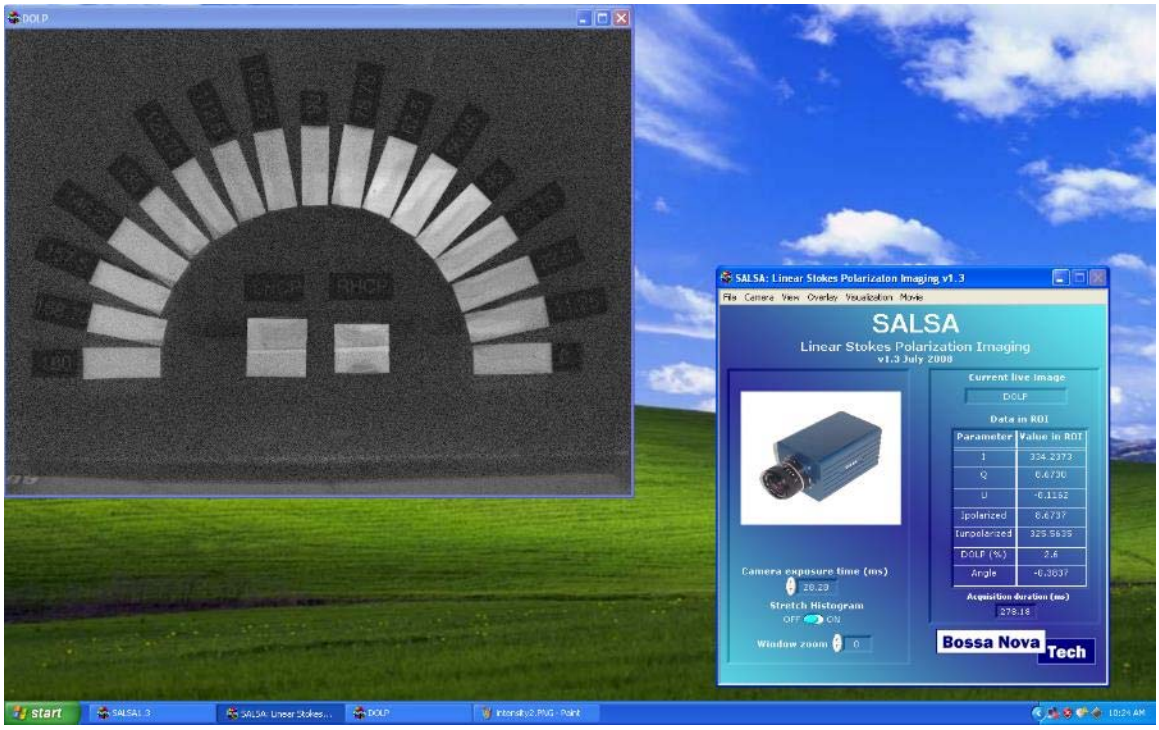

Figure 21. Salsa Software Live Imagery.

The Salsa software allows for a simple output to save all files or select certain files. The main files utilized to compute products from Stokes vectors are .txt files which contain the pixel by pixel values for I (S0), Q (S1), and U (S2). The .txt files are used in IDL to perform Stokes product representations.

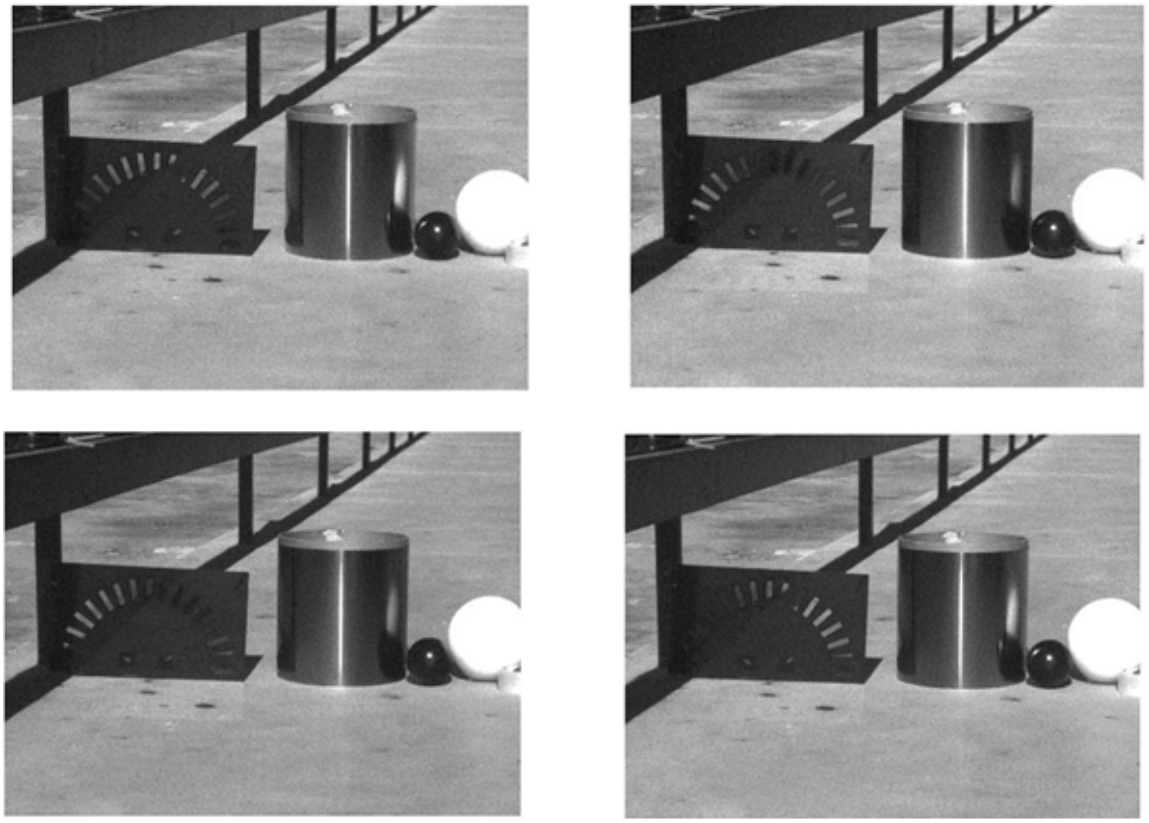

Frame 1(top left), Frame 2 (top right), Frame 3 (bottom left), Frame 4 (bottom right).

Figure 22. Salsa Polarization Filter Frames.

B. FLUXDATA

The Fluxdata FD-1665P 3 CCD Camera, displayed in Figure 23, is capable of capturing video and images at three linear polarization directions concurrently without time delay in full color. The ability to simultaneously capture imagery without sequential switching of filters eliminates timing and movement issues. This design puts more control in the user's hands and requires the user to interact more with the data to view Stokes parameters and product calculations.

Figure 23. Fluxdata Camera. Source: Fluxdata.

The camera sensor type is a Progressive Scan Charge Coupled Device (CCD) Sony ICX285 with a sensor size of 1628 x1236 pixels. At full resolution, the camera is capable of 30 frames per second. This CCD sensor converts light into electric charges that process to electronic signals for digital images. The camera offers 1.4 megapixels and an F mount lens that is interchangeable. A NIKON f/2.8 NIKKOR 28mm was used in the cameras operations. The Fluxdata comes in a compact design measuring (4.6” × 3.5” × 4.4”).

The Fluxdata features three CCD sensors on three polarizers as depicted in Figure 24. This concept utilizes division of amplitude polarimeters (DoAmP) which avoids timing issues observed using DoTP. The 3-way beam splitting prism is assembled with multiple non-polarizing beam splitter coatings. Two coatings layer the prism to split the incoming light into three components with equal spectral components. Additionally, linear polarization trim filters are positioned in front of each CCD sensor to provide spectral selectivity. DoAmP avoids timing issues by capturing images simultaneously and then splitting the beam into three equal analyzers before being refocused onto their focal planes. This results in three full resolution images that can be used to calculate Stokes vectors pixel by pixel using a modified Pickering method. The issue that arises using DoAmP is aligning the images on the focal plane because of the complex optical paths (Schott 2009, 147).

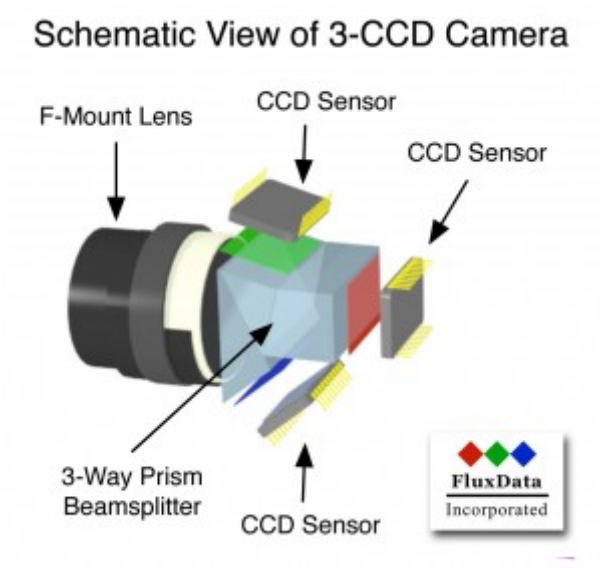

Figure 24. Fluxdata Color CCD Sensors. Source: Fluxdata.

The Fluxdata camera's polarization filters are oriented at 0, 135, and 90 degrees. Traditionally, the Fluxdata camera's polarization filters are oriented at 0, 45, and 90 degrees. The change in the 45 degree filter to 135 was discovered during testing and target detection using a polarization angle filter wheel as depicted in Figure 26. This change in filter alignment requires careful use of the 135 degree measurements, rather than the traditional 45 degree calculation. The S2 calculation appears to be an opposite image as compared to the Salsa's S2. Reversing the sign of the calculations allowed the Stokes vector calculation to produce results corresponding to those obtained from the Salsa. The ability to output data prior to Stokes calculations is a feature that is not available on the Salsa.

The Fluxdata utilized a Lenovo X250 laptop running Windows 7 with an Intel Core i5 and 8GB of RAM. The camera is powered by 8V DC ~30V DC, 840mA 12V DC (10W) via a Hirose 12-pin general purpose input-output connector trigger which can be connector to direct power or a battery pack. The camera utilizes 3 GigE (CAT 5) connections with a NETGEAR Ethernet switch to connect the channels via CAT 5 to the laptop for high speed data transfer of each channel.

The camera uses the Basler software Development Kit and View Application Field Kit, running Pylon version 4, 64 bit viewer. The typical view of the software is dislayed in Figure 25. The software supports various inputs including GigE Vision, IEEE 1394, Camera Link and USB3 Vision Standard. To communicate with the software the computer was set with a static IP on the same subnet as the camera with each channel of the camera set.

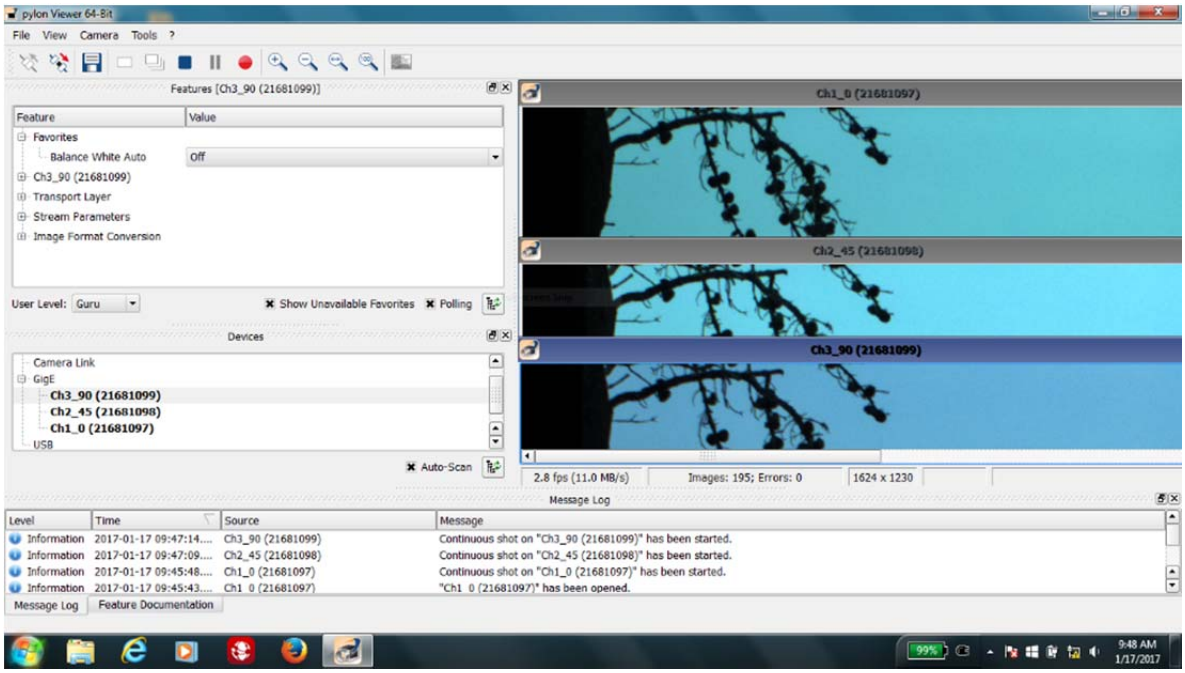

Figure 25. Fluxdata Software Interface.

The software can be operated in three modes based on the user's level of skill, from beginner, expert, or guru, as shown in Figure 26. Each level includes different options to alter to gain the best quality image and use functions such as the trigger mode.

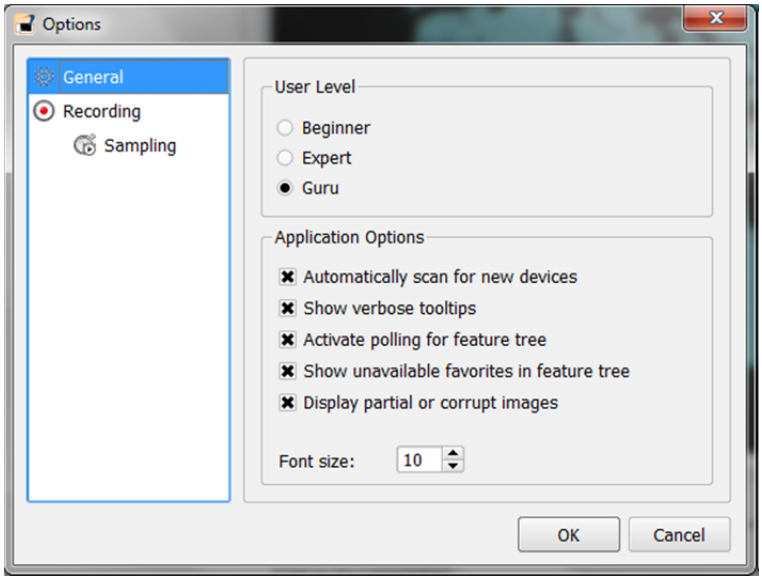

Figure 26. Fluxdata User Settings.

The output for the Fluxdata requires the user to trigger embedded software to capture three simultaneous images. To achieve a triggered result a main channel must be selected to act as the primary controller of the other two channels. Selecting the single shot button on the primary channel will trigger the other images to stop. After triggering all input channels to stop the user must individually save each .tiff file for 0, 45, and 90 degrees, as shown in Figure 27. The trigger software and settings do not work every time and a closer analysis must be completed by comparing and registering the photos after saving them. If the trigger mode was unsuccessful the images results cause errors in registration. An attempt at creating a standard operating procedure was made but resulted in errors on certain occasions. The exact cause of the trigger mode error was not determined.

The Fluxdata does not perform any computations of Stokes vectors or products. Only the live images and video of 0, 45, and 90 degree polarization filters can be viewed while setting up and preparing a capture. Computation of Stokes must be completed after saving the .tiff files using IDL or MATLAB to compute each pixel to Stokes.

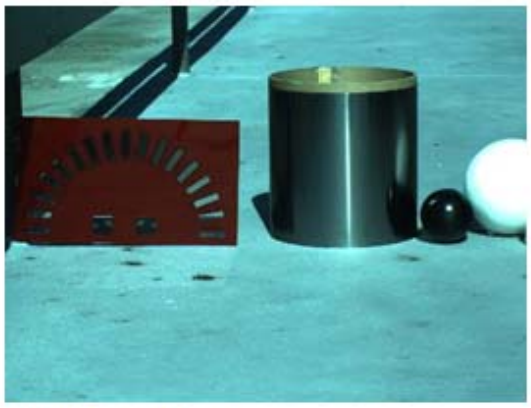

Channel 0, 0 degree

Registered 0 degrees

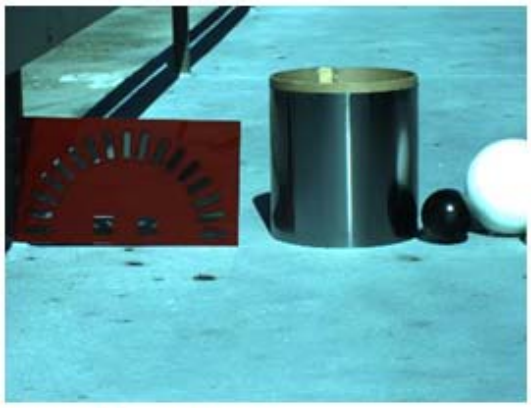

Channel 1, 45 degrees

Registered 45 degrees

Channel 2, 90 degrees

Registered 90 degrees

Figure 27. Fluxdata Input/Output Channels (left) and Registered Images (right).

Each channel offers a set of features to control analog and digital controls of the process as displayed in Figure 28. The ability to manipulate each channel gives the user much control to counter the effects of gain and saturation effects.

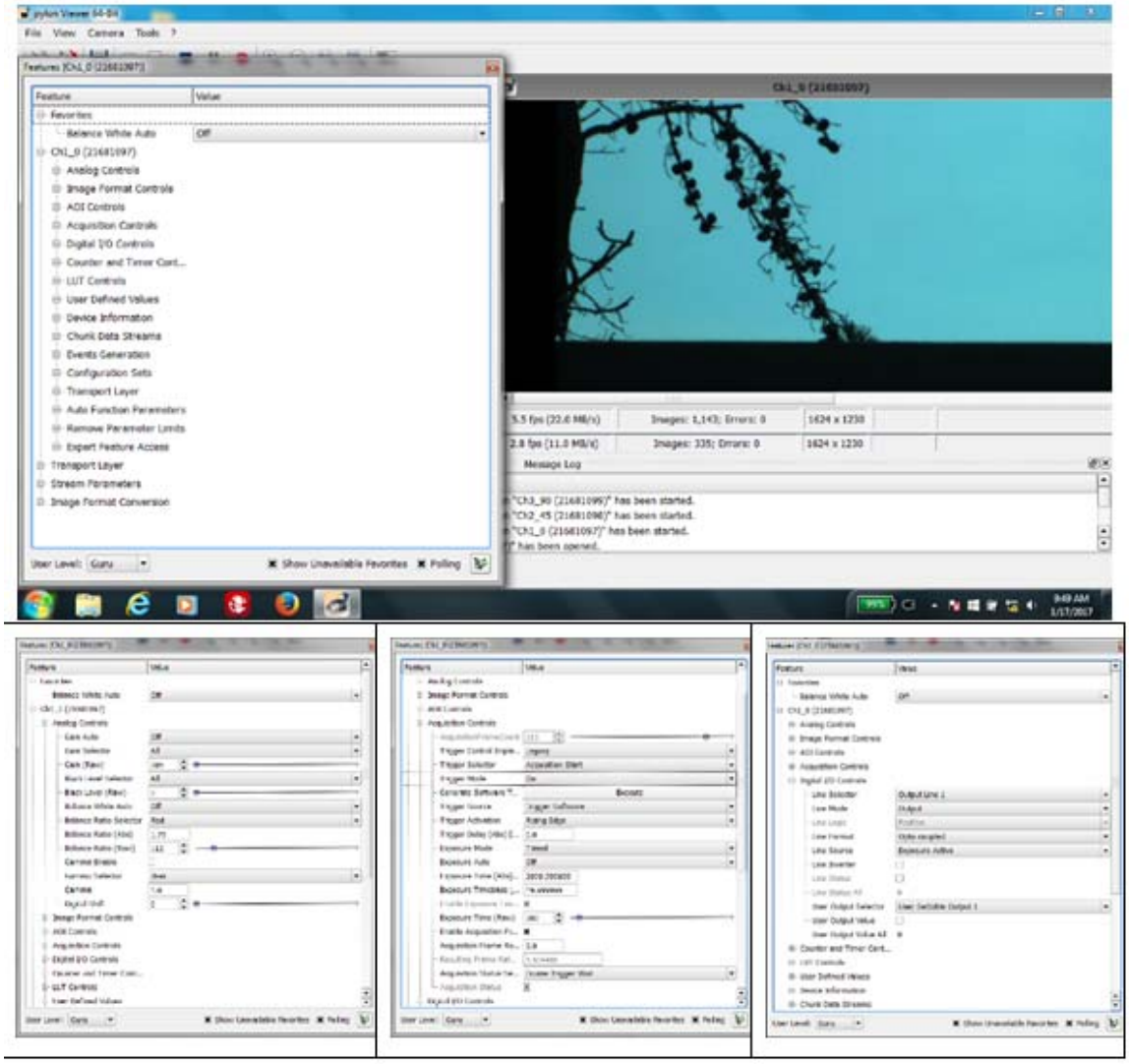

Figure 28. Analog Functions, Acquisition Controls, and Digital I/O Controls.

THIS PAGE INTENTIONALLY LEFT BLANK

IV. METHODOLOGY

The method of capturing images consisted of mounting both cameras on tripods at similar angles to the scenes being captured, as shown in Figures 29 and 30. The images were taken at approximately the same time to obtain results from a similar sun angle. Although the results are slightly different when viewing the imagery in respect to size, resolution, and quality, the larger aspect of determining how the cameras determine polarization are compared using ENVI.

Figure 29. Camera Setup.

The comparison of the cameras and images followed the method of testing used in modern day cameras on phones. Concepts of the ease of use, quality of photos, cost, support, and various details are analyzed to determine the best use of each camera and how a customer would best utilize this emerging technology.

Figure 30. Initial Test.

To compare the images, the software program ENVI 5.3 (Environment for Visualizing Images) was used, along with IDL 8.5 (Interactive Data Language) to manipulate the raw data to create and view Stokes vectors and products. ENVI by Harris is software that does image processing and analysis for remote sensing. Functions in ENVI such as band algebra and histogram manipulation were used to compare the Fluxdata and Salsa images. IDL is a programming language that was used to process the .tiff images to create Stokes parameters. Prior to using ENVI or IDL, the Fluxdata images were converted to grayscale and then registered using MATLAB in order to use IDL to convert the polarized images to Stokes measurements.

The total intensity captured by both cameras varied greatly and manipulation of the histogram scale in ENVI was utilized to scale the image and eliminate noise and saturation.

V. DATA ANALYSIS

The data was analyzed both qualitatively and quantitatively using ENVI. Various scenes of the Naval Postgraduate School Campus and downtown Monterey, California were captured between July and December of 2016. When viewing the images, a color representation is displayed following columns of images from the Fluxdata and Salsa. After a comparison of the two cameras, the Fluxdata images are displayed with the three Stokes representations and DoLP.

When viewing the grayscale images, the intensity is represented by the brightness of the image. For example, S1 image is brighter in the horizontal 0 degree polarization, and darker in the vertical 90 degree angle, with gray colors not having a strong signature in either direction. Additionally, various issues with gain and oversaturation are a problem with both the Salsa and Fluxdata and can be seen in certain objects. IDL was utilized to scale the images and remove the oversaturated data.

Viewing the Stokes vectors in grayscale portrays the stronger signatures in either white or black, with gray representing electric fields received without a distinct polarization state. S0 represents the overall intensity in grayscale, basically a camera without polarization filters and does not represent any differences between polarizations. S1 displays brighter white positive value as horizontally dominating, while black negative value is vertically dominating, with gray values not having a strong signature. Similarly, S2 displays brighter white as +45 dominating and darker black values stronger in 135 degree dominating. Finally, DoLP scales the polarization from bright white as 100% linear polarized to dark black as 0% linear polarized.

The first objective in comparing the cameras was to compare the Stokes images. The resulting calculations from each camera portray similar results, shown in Figure 31. A polarization angle wheel, which consisted of polarized film arranged at angle from 0 to 180 degrees helps verify the angles of polarization being filtered. The images were taken at 1158 PST on 06 October 2016. Alongside the wheel, is a cardboard circular cutout wrapped in a highly reflective metal sheet, followed by a bowling pin and a white

Styrofoam ball. The Fluxdata displays a higher resolution image with more detail as compared to the Salsa Stokes. An advantage in the Fluxdata is the detail and differences captured in the background. The brighter portions of S1 signify stronger polarization in the horizontal field, while darker portions of the grayscale images indicate vertical polarization. Similarly, brighter portions of the S2 image show +45 polarization while darker show -45(135) polarization. The DoLP is the main product from the Stokes that helps determine how polarized the contents of an image are. Brighter portions confirm a higher percentage of polarization and darker (black) portions show no polarization signature. Using the polarization filter wheel as a starting point confirms the signatures of the Stokes images and gives a reference to refer to when viewing scenes to detect polarized items of interest. The static target confirms that both cameras calculate and portray Stokes vectors correctly and give a reference for future analysis.

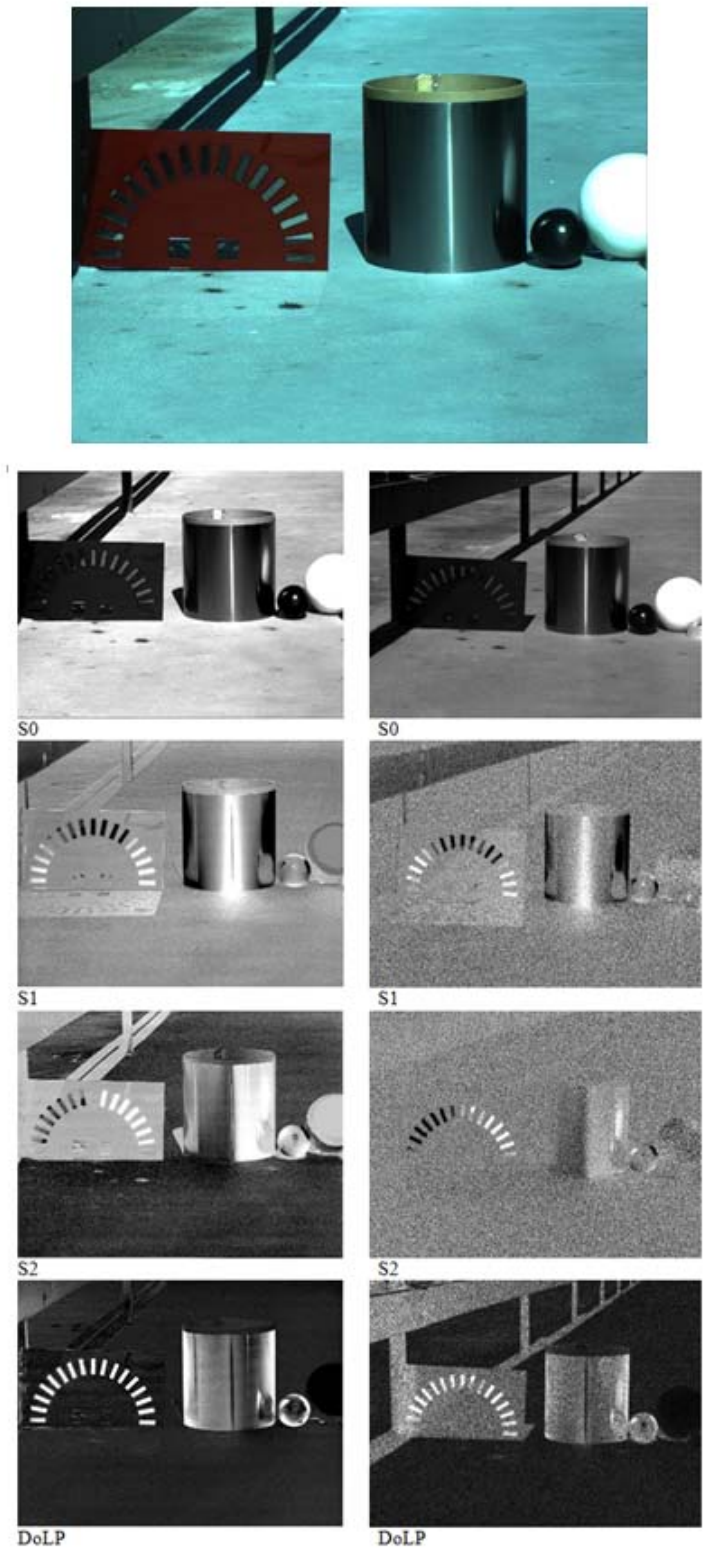

Figure 31. Target. Fluxdata (left) and Salsa (right).

The first comparison begins with Hermann Hall on the campus of the Naval Postgraduate School. The scenes in Figure 32 were captured at 1620 PST on 08 September 2016. Both cameras display similar polarization signatures in S1, S2, and DoLP when viewed in their entirety. It is easier to distinguish and identify objects in the Fluxdata. Differences in the cars and windows make them easily visible based on their polarization signature. When zooming in and comparing values of DoLP the Fluxdata gives higher values on objects such as windows and cars; shown in Figures 33, 34, and 35. The Salsa loses much of this detail when zooming in on an object. The DoTP of the Salsa is affected by movement and gives false data for moving objects such as trees. Fluxdata's DoAMP is not affected by movement of trees but registration errors do occur from very small errors in the alignment of the frames on the camera in shadows and along some objects outlines. The Fluxdata best displays differences in S1 and S2 to determine which polarization signature is strongest and help classify objects with more accurate data. The DoLP image best portrays the highly-polarized cars on the bottom of the scene.

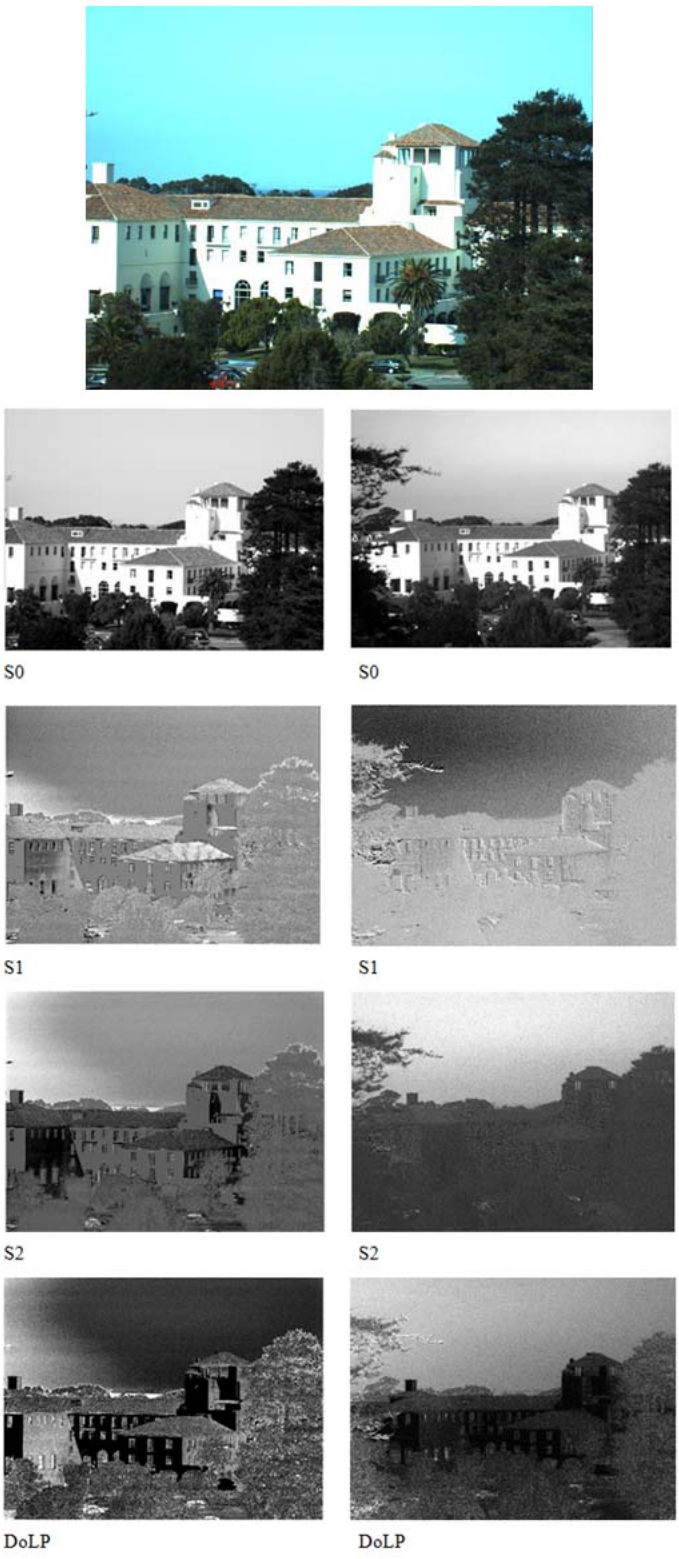

Figure 32. 08 September 2016. Hermann Hall, Monterey, CA. Fluxdata (left) Salsa (right)

Figure 33. S0 Zoomed-in Cars. Fluxdata (left), Salsa (right).

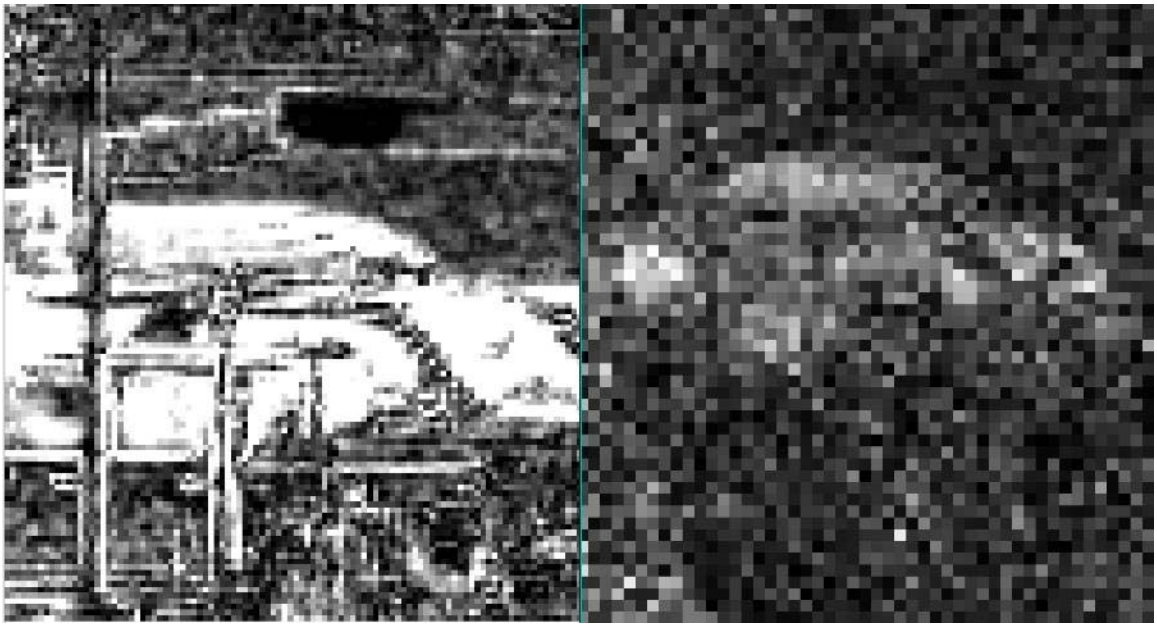

Figure 34. DoLP Zoomed-in Cars. Fluxdata (left), Salsa (right).

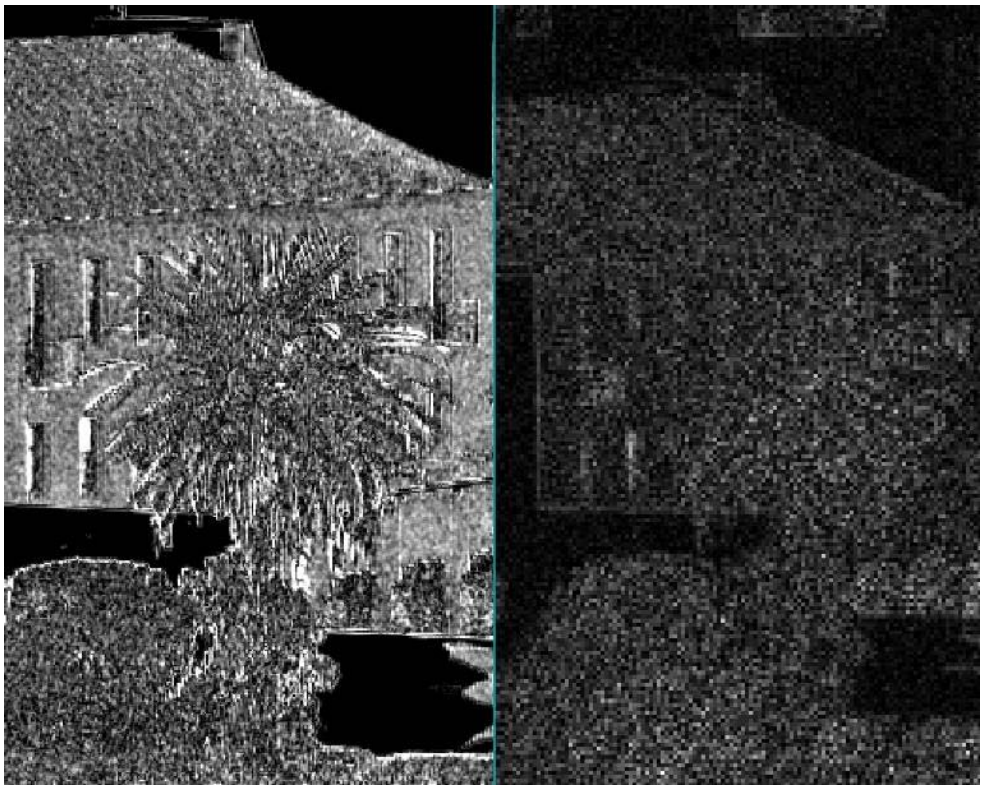

Figure 35. DoLP Palm Tree Zoomed In. Fluxdata (left), Salsa (right).

The Fluxdata's color capability adds an additional way to view polarization in color because of its red, green, and blue channels. A Hermann Hall illustration from 20 May 2016 is shown in Figure 36. The day was slightly overcast, but these data are useful here because camera saturation issues were not a problem in these data. A display of S0, S1, S2, and DoLP in color is displayed in Figure 36. The presence of color in the S1 and S2 frames indicates that there is a variation in polarization with wavelength, as might be expected. In particular, the sky varies in polarization. Limited analysis of the color dependence for the polarization signatures was done, but the issue of saturation at some wavelengths made it difficult to pursue.

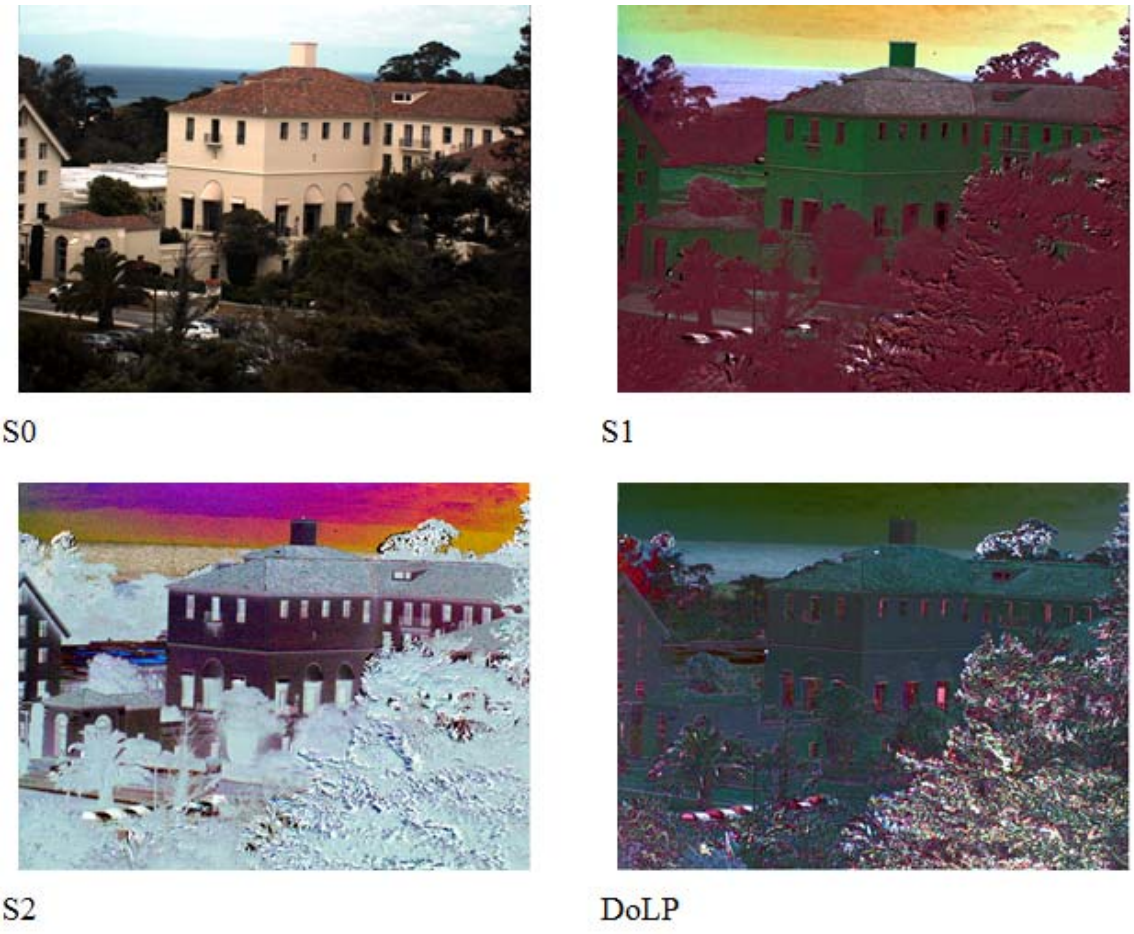

Figure 36. 20 May 2016. Hermann Hall, Monterey, CA.

The next data in Figure 37. were collected on 01 December 2016 at 1226 PST on the rooftop of the Marriot Hotel in Monterey, CA. The scene captures a portion of the Monterey harbor and an adjacent building. It is apparent to see the advantage of the Fluxdata's DoAmP technique, shown in Figure 39, with the moving seagulls in the top right portion of the Fluxdata. This technique is an advantage over the Salsa because it is not affected by movement which causes registration errors and false data on polarization signatures, as seen in Figures 38 and 40. Although these images do not portray any major object identification from their polarization, the Fluxdata again captures more detail and is not as affected by the background saturation.

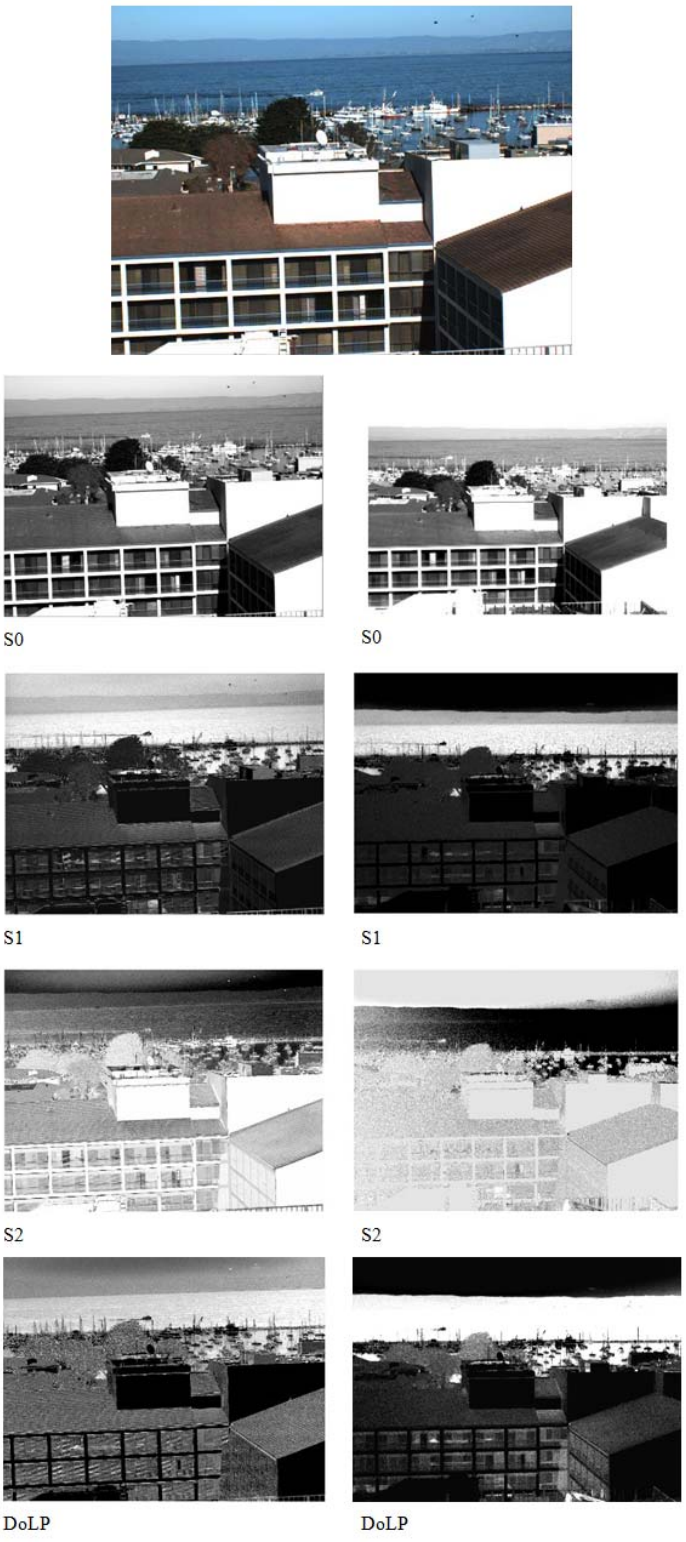

Figure 37. 01 December 2016 Marriot rooftop. Fluxdata (left), Salsa (right).

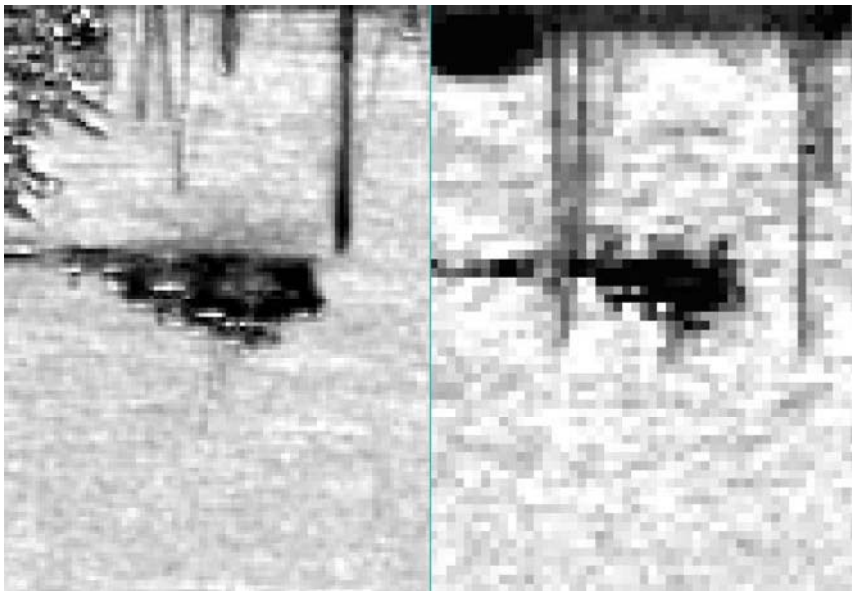

Figure 38. Moving boat on water. Fluxdata (left) Salsa (right).

Figure 39. Seagulls. Fluxdata.

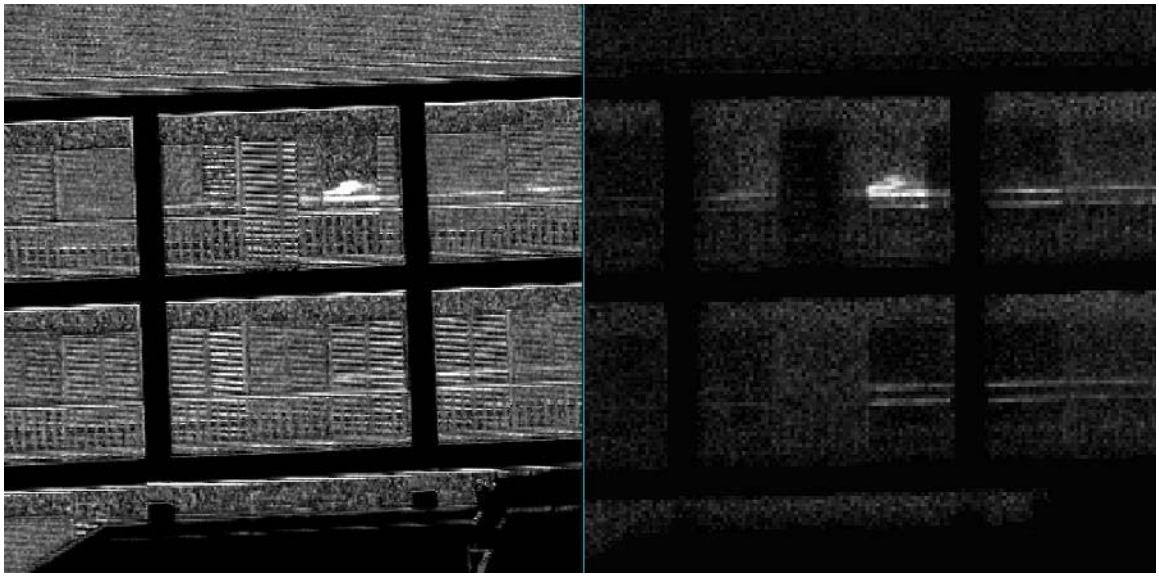

Figure 40. Blinds in windows. Fluxdata (left) Salsa (right).

The next scene, in Figure 41, was a construction site captured on 01 December 2016 at 1215 PST. The scene had many moving features and items of interest to include wood, metal structures, construction equipment, dirt, gravel, power cables, and people. The Fluxdata's technique of capturing polarization was not affected by the moving aspects of the scene and highly polarized objects such as the windows on a truck and some reflective material on a ledge are distinguishable. The power cable did not show any distinguishable polarization signature and is difficult to detect in any of the Stokes images.

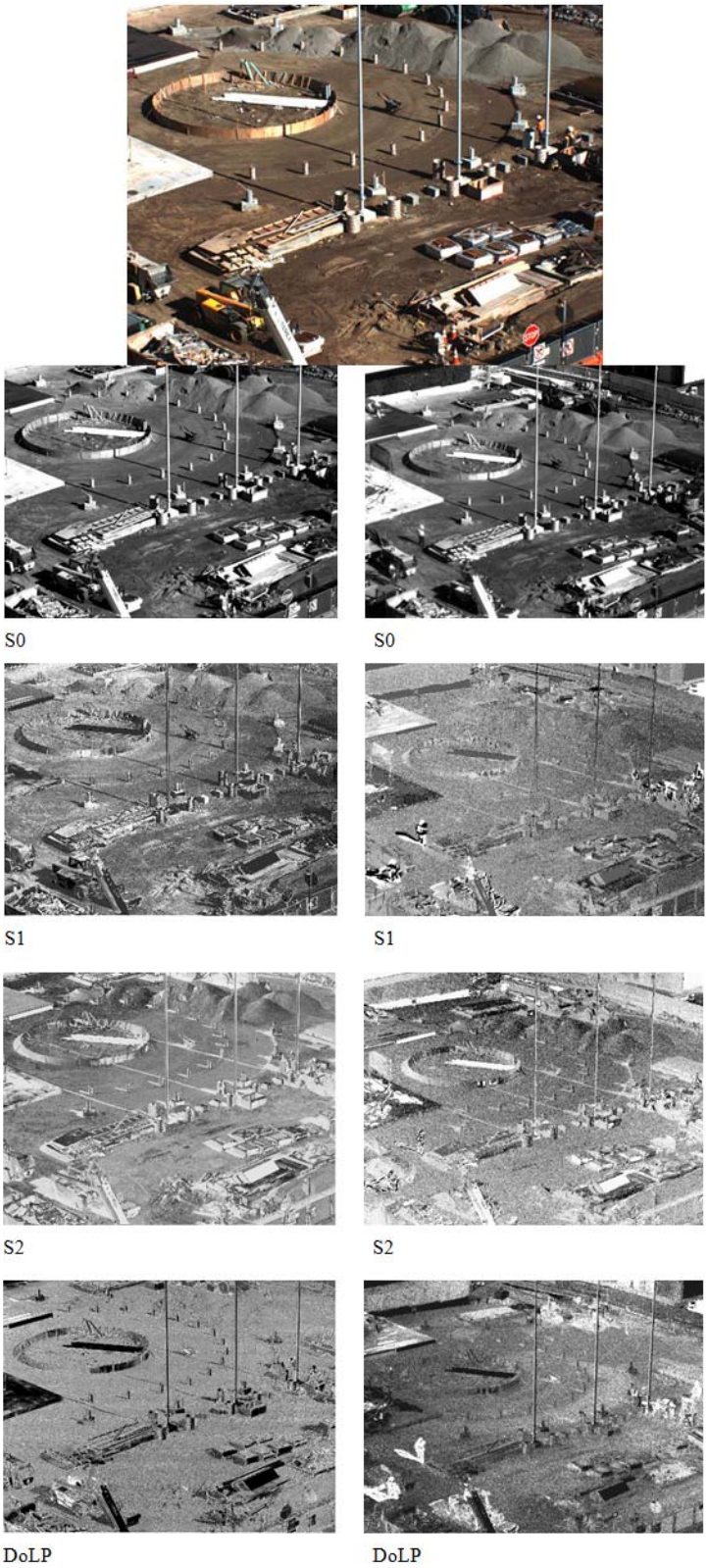

Figure 41. 1 December 2016. Construction Site. Fluxdata (left) Salsa (right).

The remaining analysis focused on the Fluxdata and capturing scenes to expand on potential uses in remote sensing. The Fluxdata's higher resolution and DoAmP display a more accurate pixel calculation of Stokes vectors in moving scenes. For example, trees and their movement are not as affected as they are with the DoTP in the Salsa. In addition to the DoAmP, the Fluxdata captures a color image and the UMOV effect is explored to see how wavelength and color affect polarization for its use in classifying objects.

The scene in Figure 42 consisted of a camouflage covering placed over a car to see how camouflage affects polarization. The cars and their windows all display a high polarization signature but the camouflage masks the signature and lowers the degree of polarization. Much of the light captured in the imagery appears to be partially polarized. The camouflage's DoLP is lower and closer to the signature of the trees, as seen in Figure 43. The ability to hide in plain sight is a polarization technique some fish use to hide in the ocean and shows how camouflage can be used to mask metallic objects (Brady 2015).

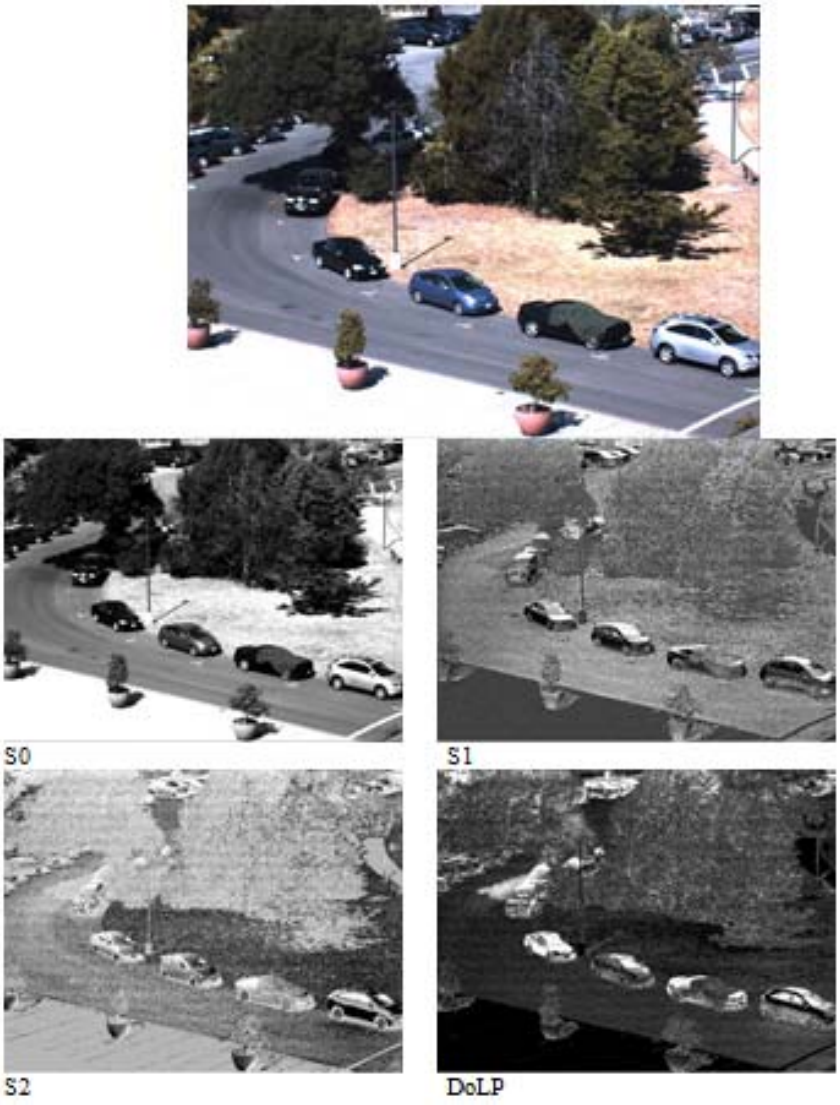

Figure 42. 26 September 2016. Fluxdata Camouflage on Car Scene.

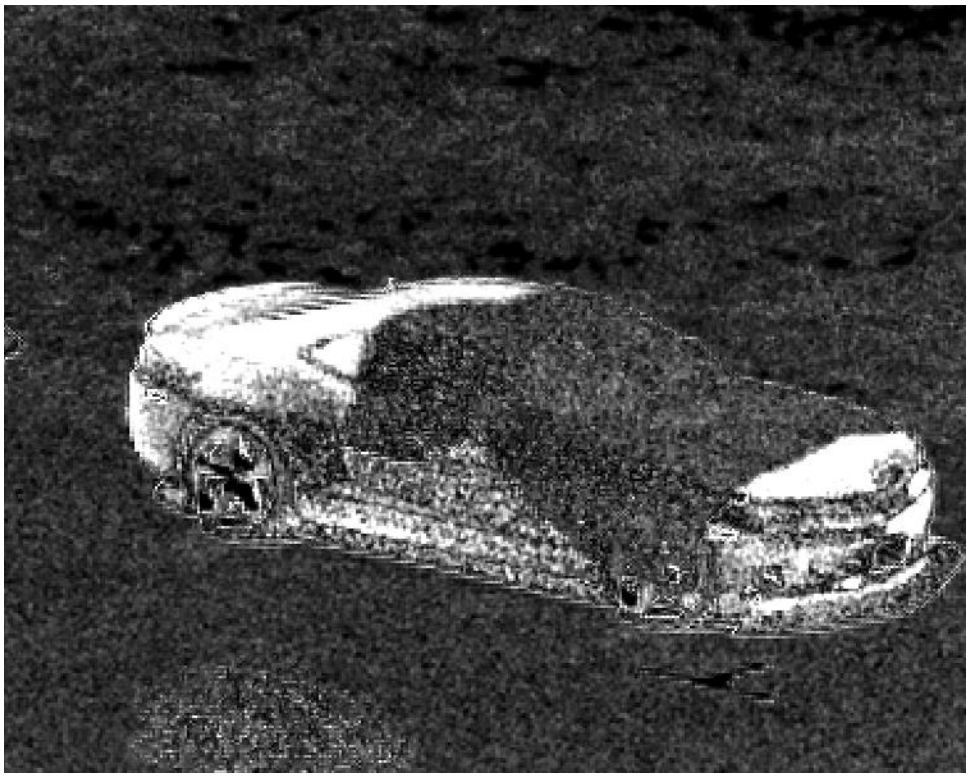

Figure 43. DoLP Camouflage On Car.

A picture of a magnolia tree and a bare tree in Figure 44 was taken at 1154 on 26 September 2016. The image portrays a mixed degree of small linear polarization signatures and does not contain any major observable artifacts. The small registration errors cause miscalculations in Stokes values.

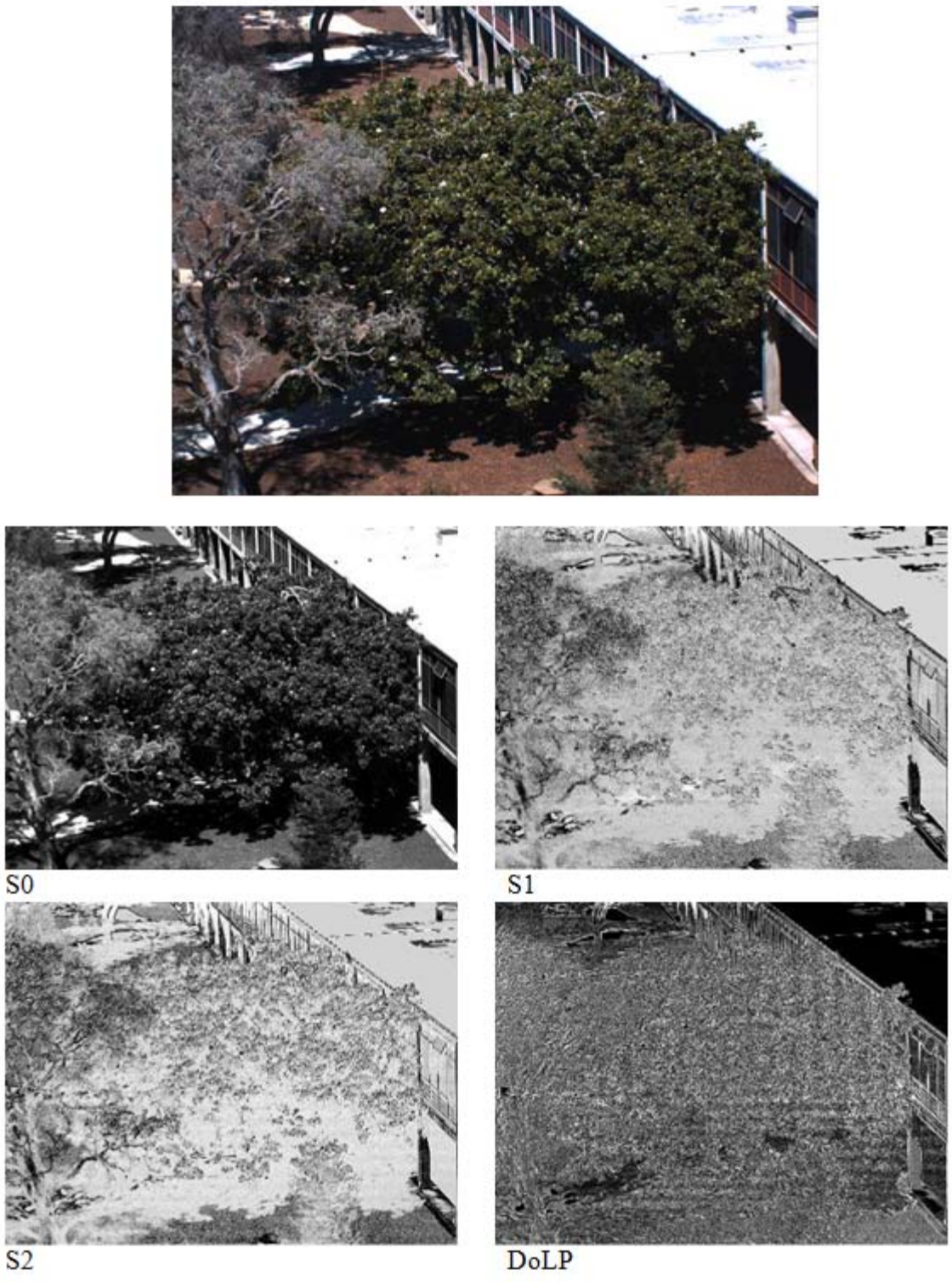

Figure 44. 26 September 2016. Magnolia tree.

The scene in Figure 45 was taken on 08 July 2016 at 1527 PST. The scene contains a large vegetation and building combination with a large arrangement of power lines and wires connecting on top of the building and in the background. The power lines in Figure 46 are more easily viewed in the Stokes DoLP representations.

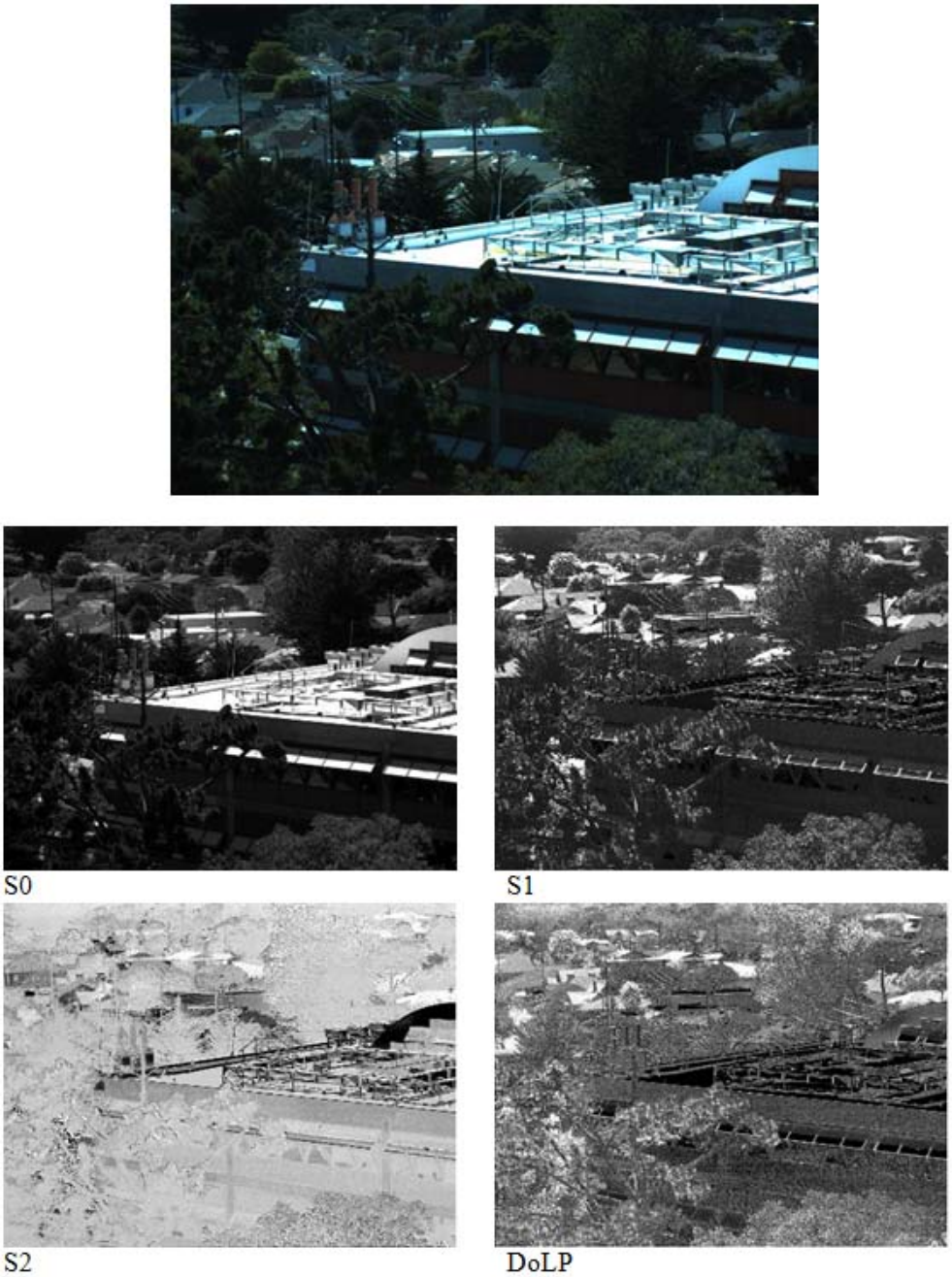

Figure 45. 08 July 2016 Bullard Hall, Monterey, CA.

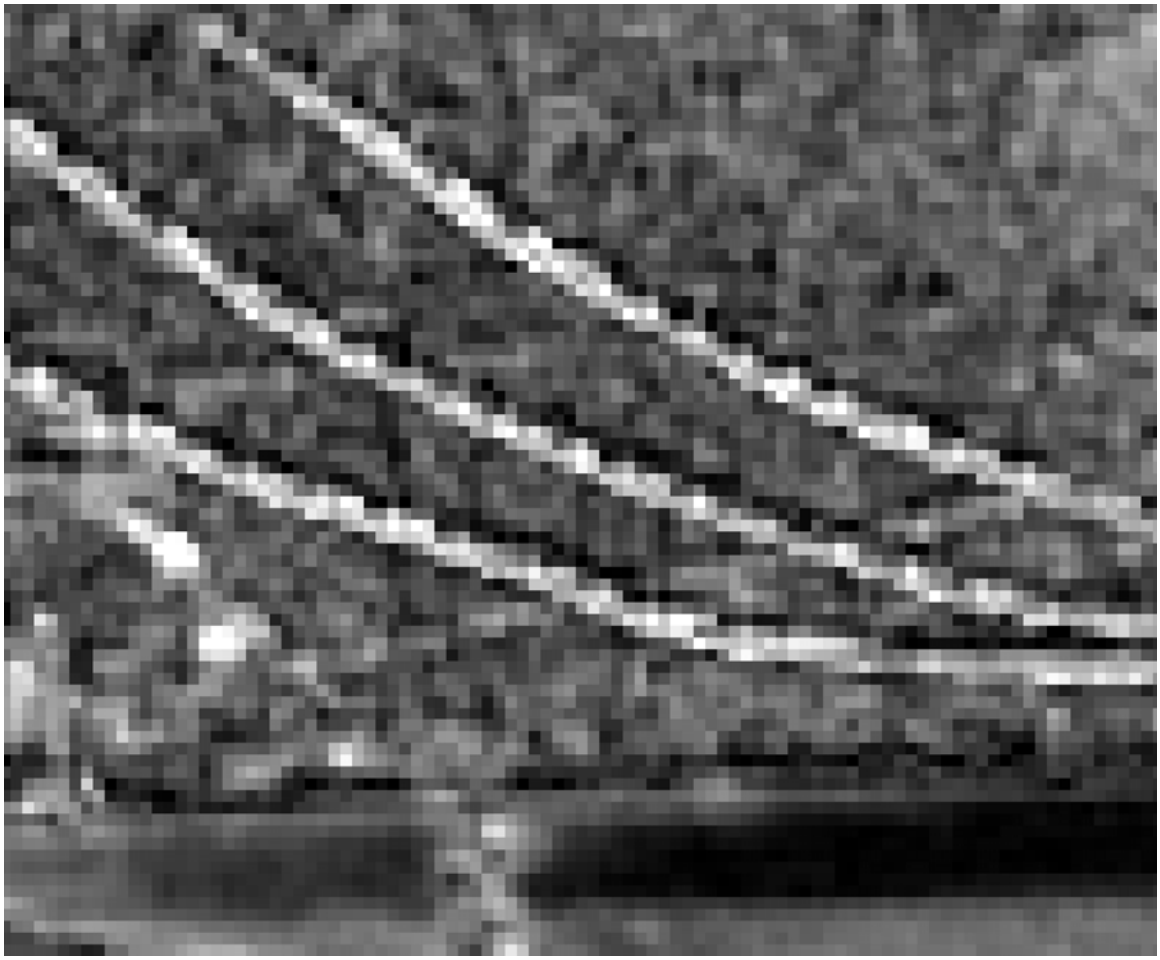

Figure 46. DoLP Zoomed-In Powerlines.

The UMOV effect was explored in the construction scene and various other scenes by creating regions of interest in ENVI and comparing their DoLP and Inverse Intensity. The assumption was the Fluxdata's color filters would show the relationships between color, DoLP, and the inverse intensity. Careful analysis showed little evidence of the UMOV effect in the data.

VI. CONCLUSION AND RECOMMENDATIONS

The Salsa and Fluxdata cameras both provide similar polarization representations. The comparison of the imagery confirms polarization signatures and the calculation of correct Stokes vectors and products. The Fluxdata's division of amplitude polarimeter minimizes the effects of false polarization because of scene movement (Goldstein 2003, 389). The advantage of this technique over the Salsa's division of time polarimeter allows the camera to be used on moving vehicles and aircraft because it is not affected by a rotating filter to calculate Stokes. Additionally, the effects of moving trees and objects in a scene can be correctly captured and calculated. The Fluxdata's focal plane alignment causes small registration errors that may need to be adjusted.

A concern in the field of polarization is the lack of data and scenes to be analyzed to determine its best use of polarization for remote sensing. Appendix A includes numerous scenes displaying Stokes images to help expand the library of polarized images for remote sensing. The uses of polarization in remote sensing will continue to grow as more objects and scenes are explored.

The limitations of imaging polarization include sun angle, clouds, saturation, and registration errors. The Fluxdata removes the concern of movement and in future work the DoAmP technique can be used on ground and air vehicle to capture overhead angles to help expand the library of polarization scenes.

The addition of color in polarimetric imaging may be prevalent in target detection and classification based on the wavelength and signature. The UMOV effect has been explored to show a relation in the wavelength with the Fluxdata's color capability. This relationship was not conclusive to display the UMOV effect and needs to be further studied to determine its use in object classification and target detection.

Finally, the Fluxdata has the capability to calculate Stokes in real time with software and code implementation. Future work with real time imagery will allow the user to select areas of interest easier and adjust angles to best capture a scene and identify objects.

THIS PAGE INTENTIONALLY LEFT BLANK

APPENDIX A. FLUXDATA IMAGES

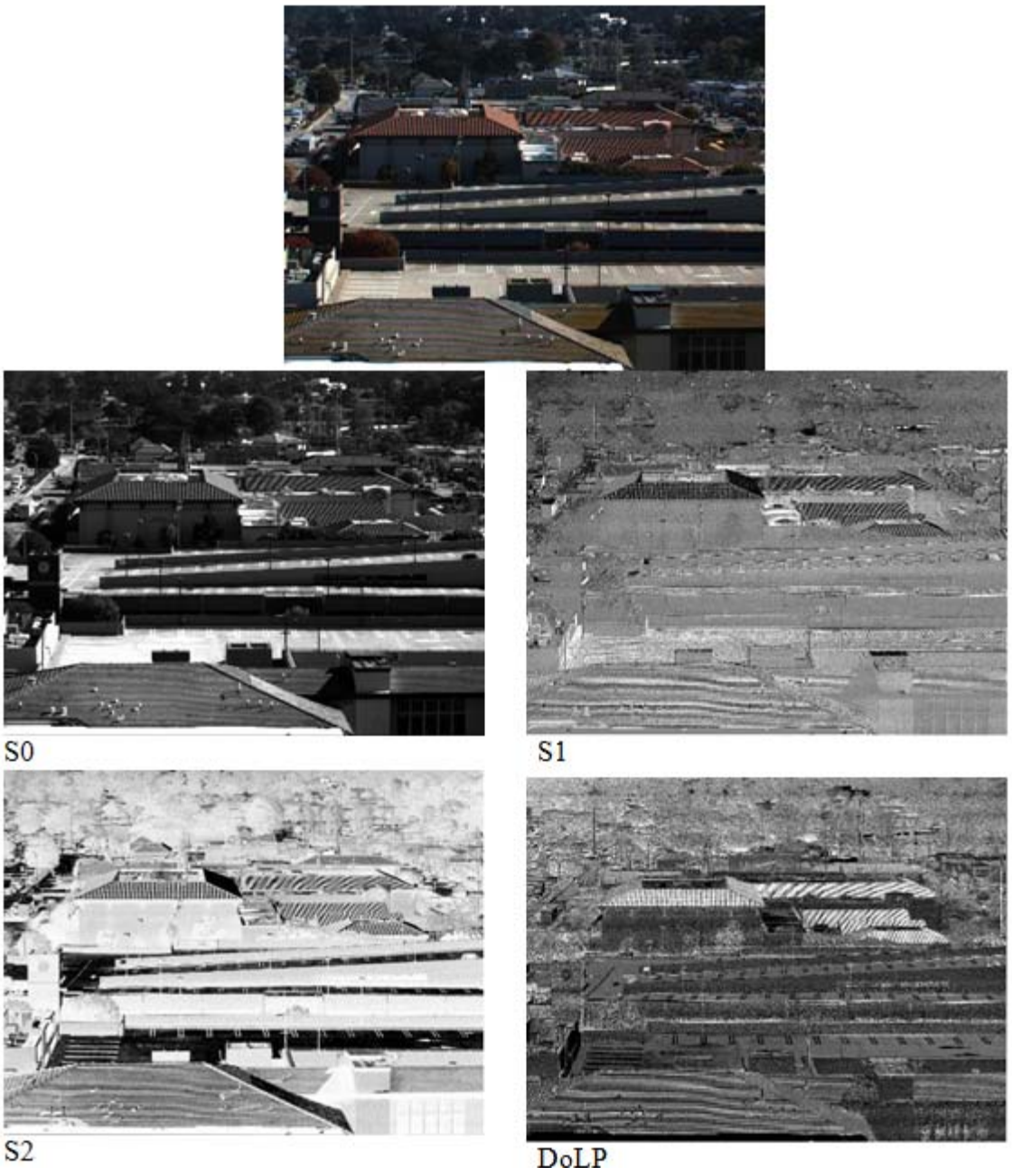

Figure 47. 01 December 2016, 1147 PST.

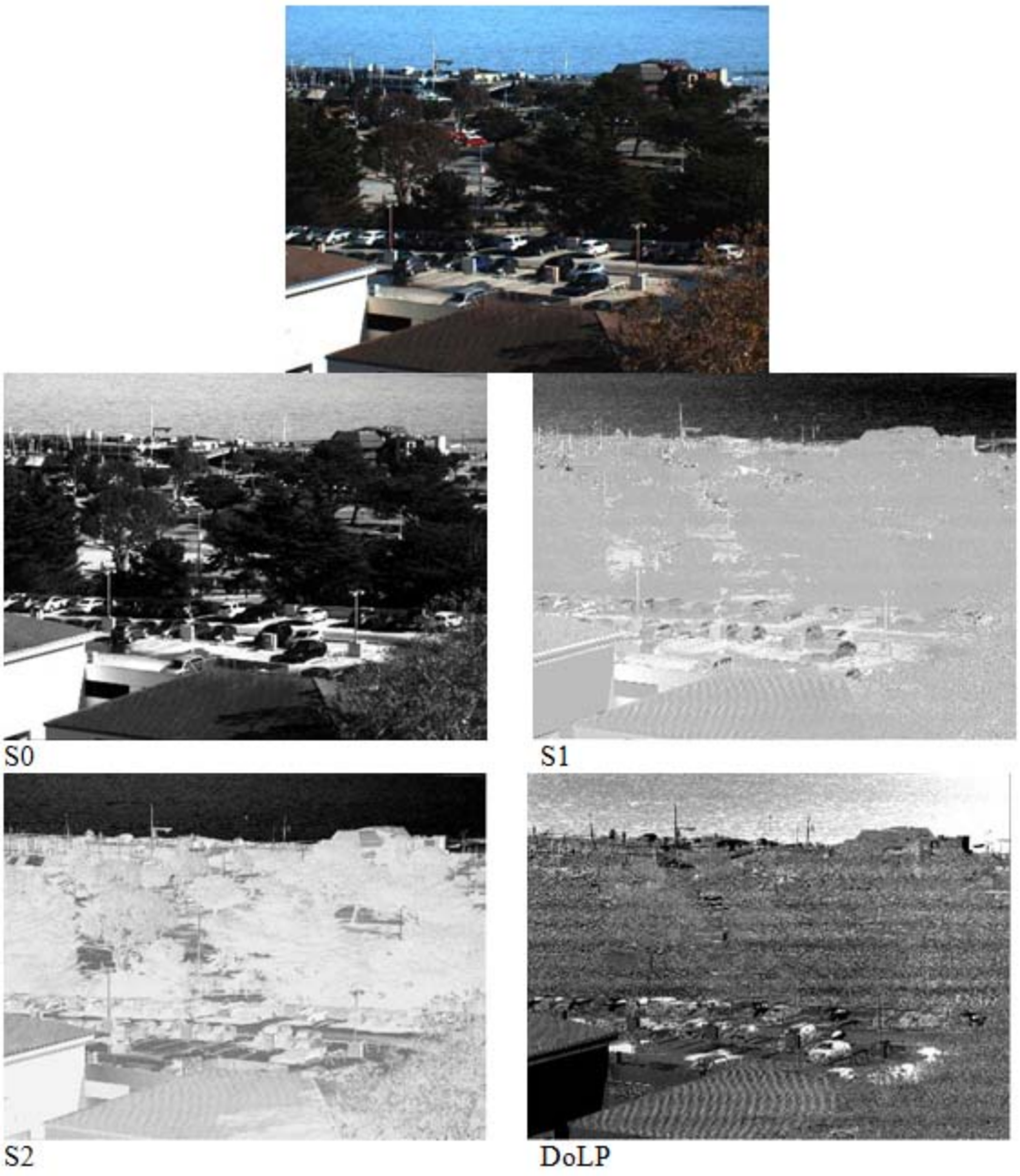

Figure 48. 01 December 2016, 1200 PST.

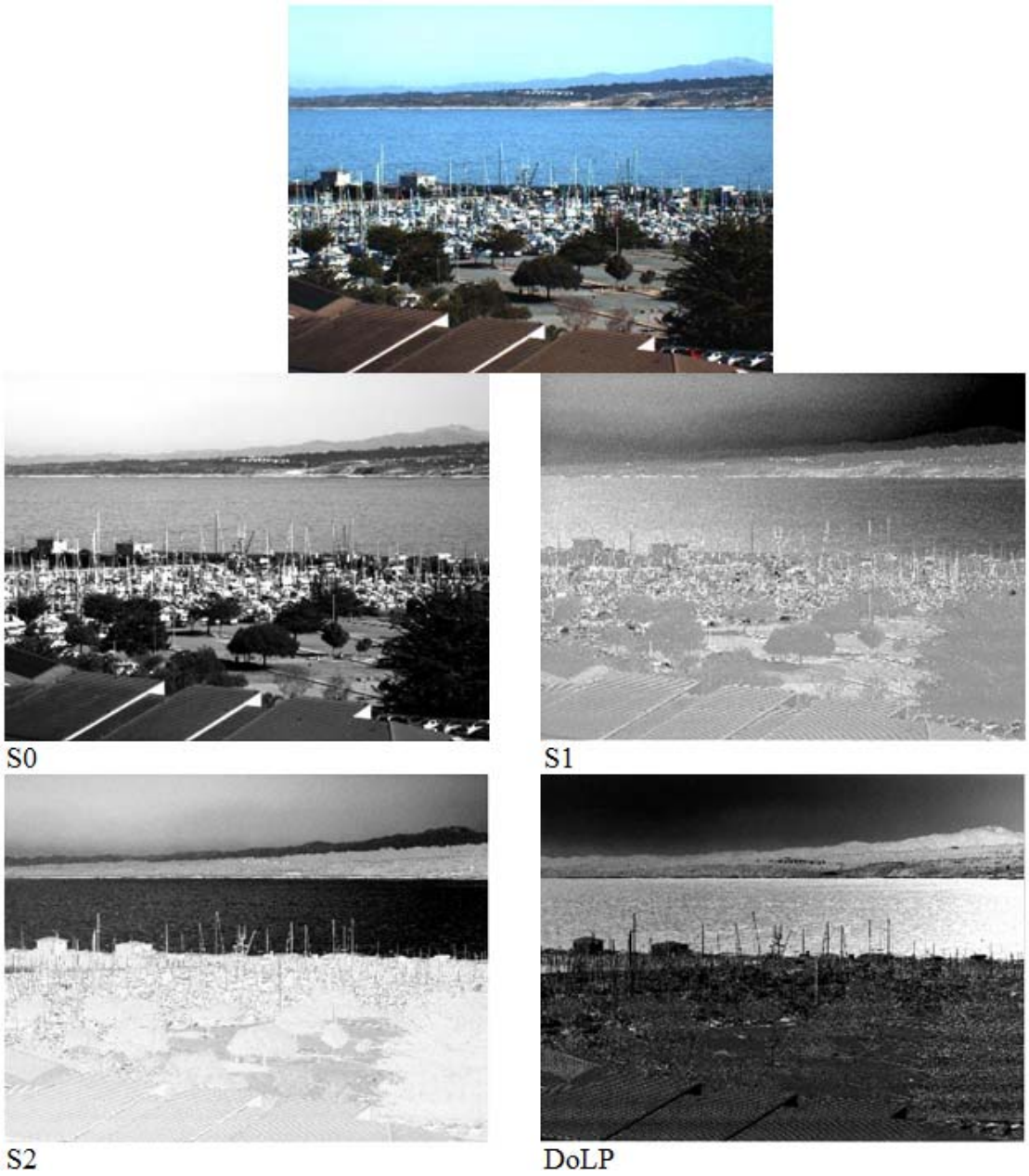

Figure 49. 01 December 2016, 1208 PST.

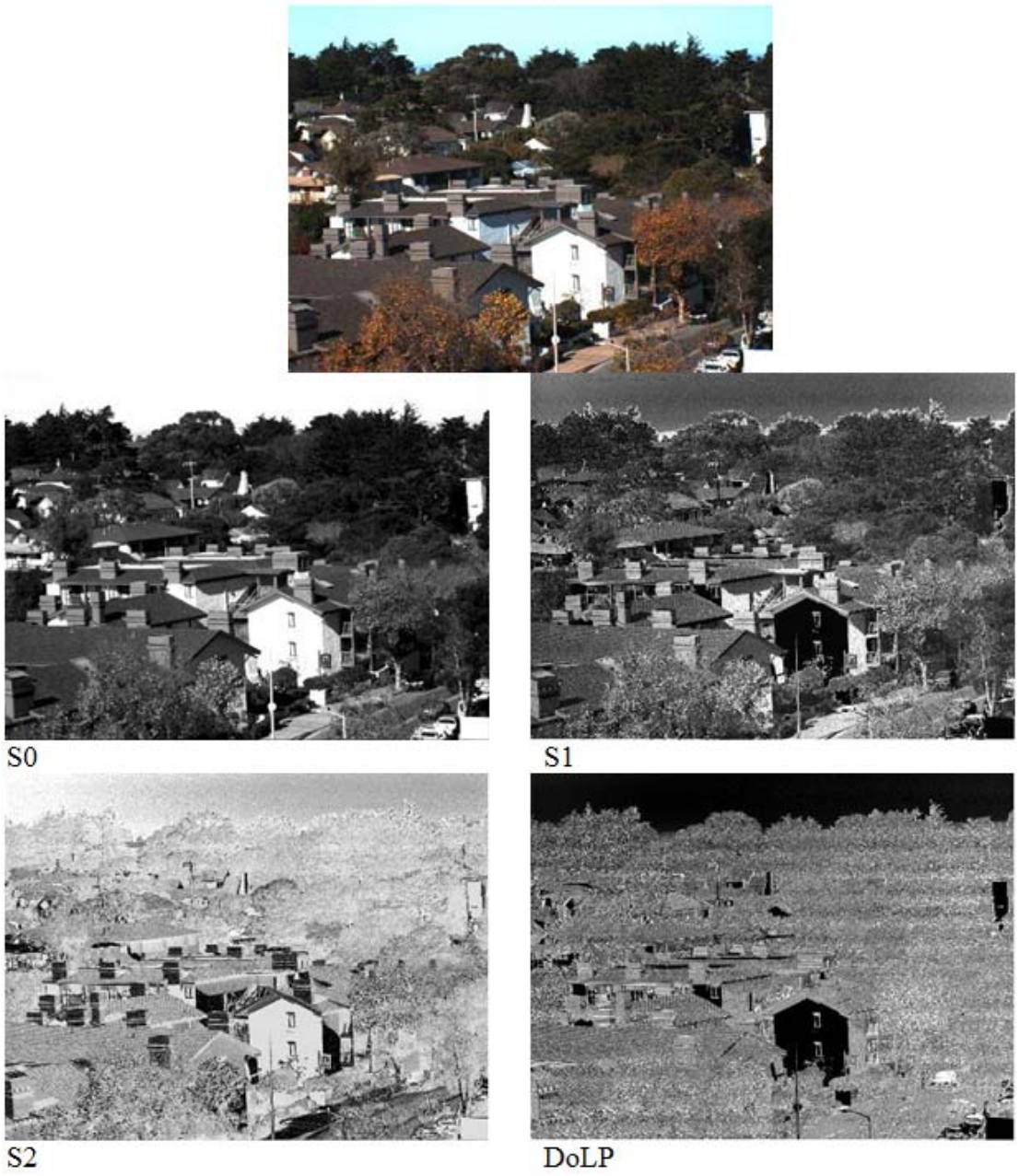

Figure 50. 01 December 2016, 1223 PST.

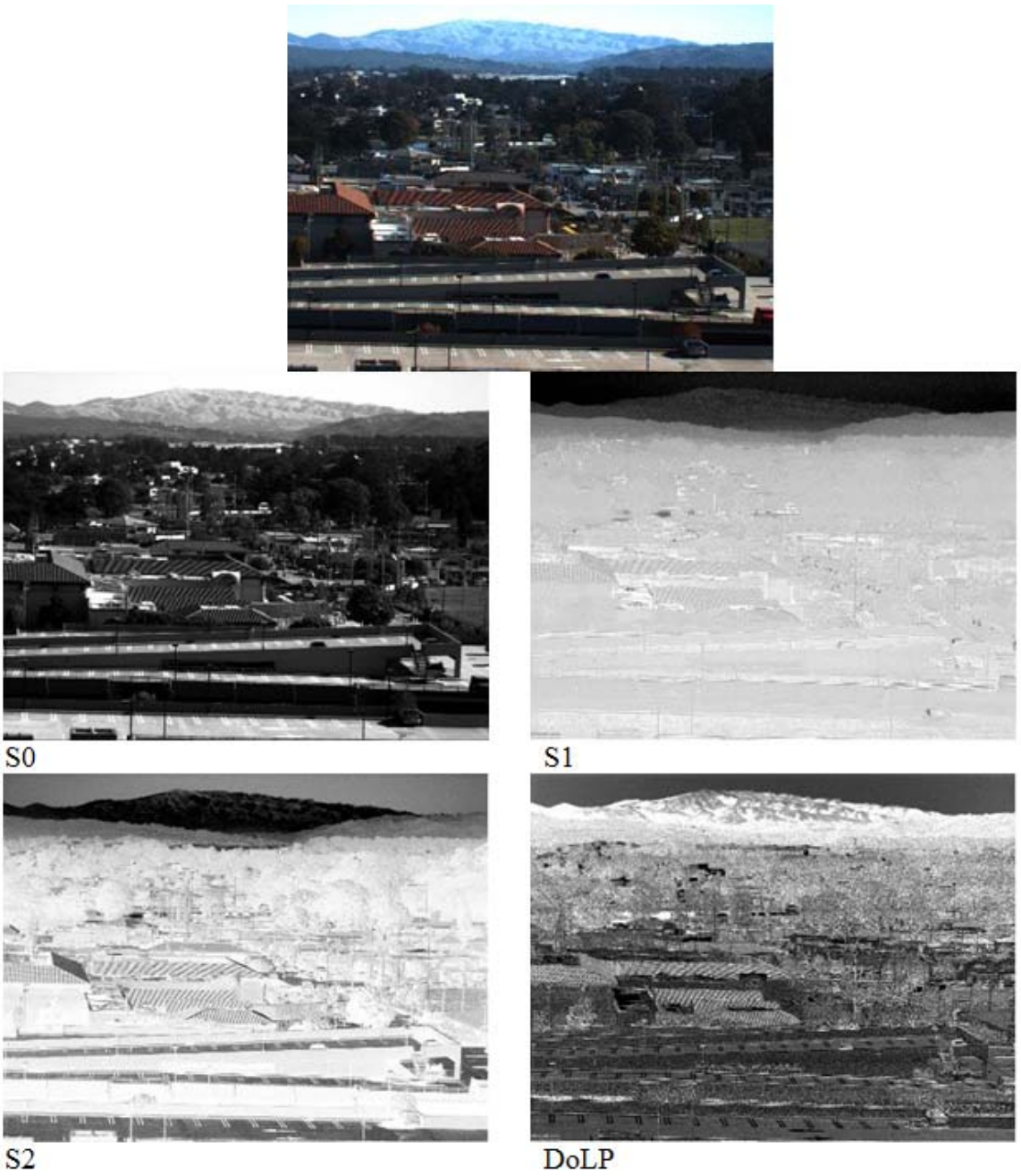

Figure 51. 01 December 2016, 1237 PST.

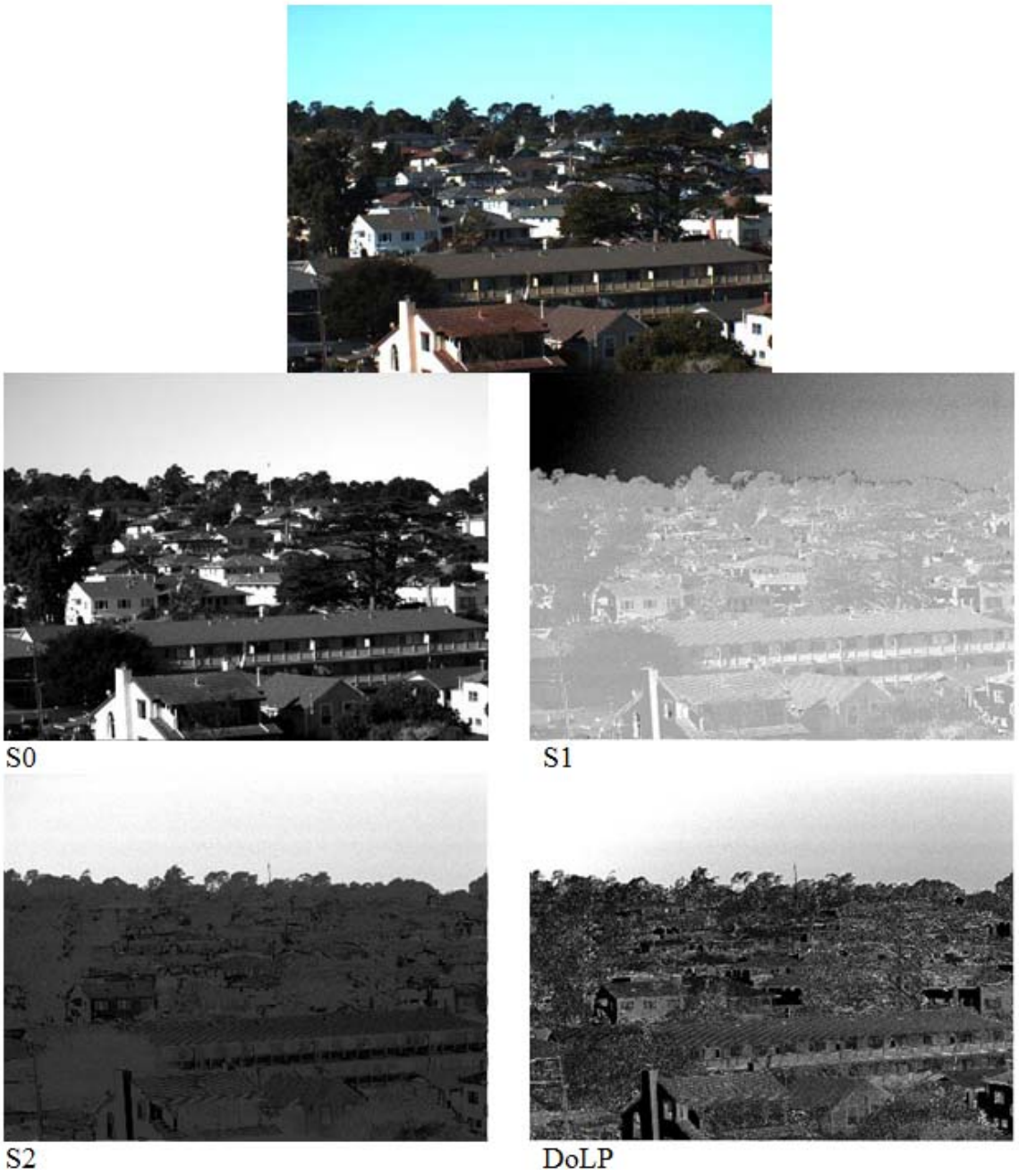

Figure 52. 01 December 2016, 1242 PST.

Figure 53. 01 December 2016, 1305 PST.

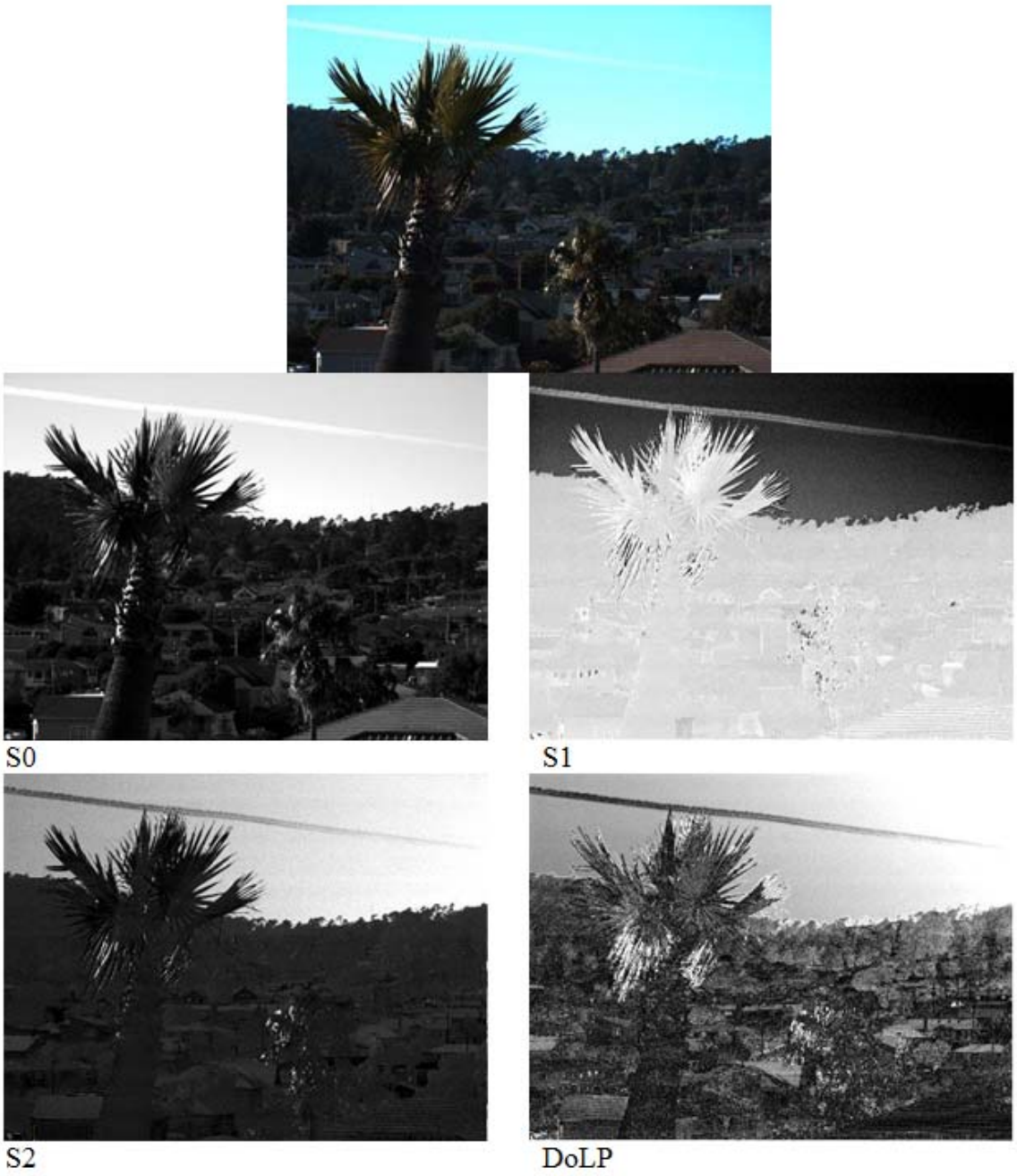

Figure 54. 01 December 2016, 1312 PST.

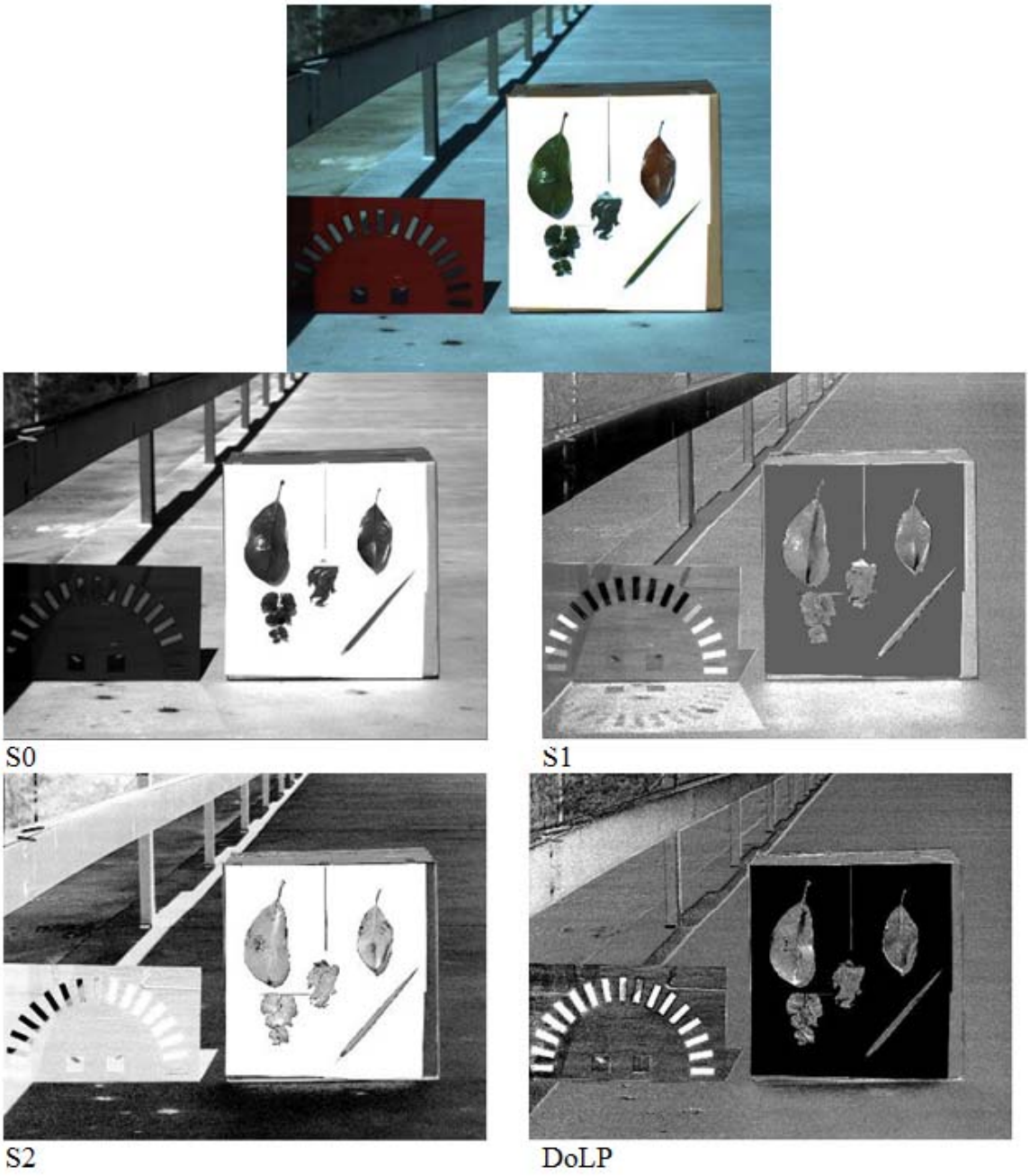

Figure 55. 06 October 2016, 1238 PST.

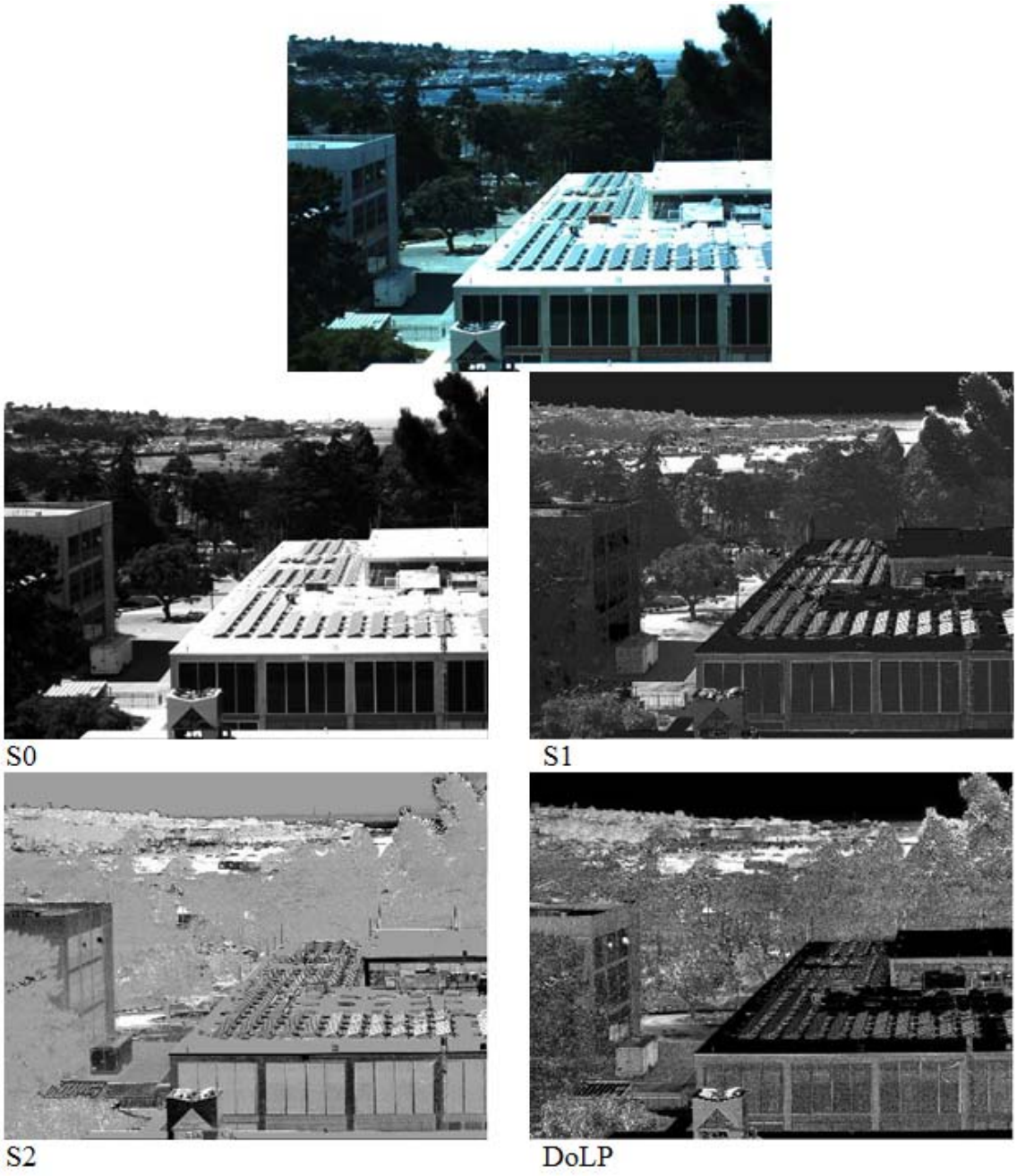

Figure 56. 08 July 2016, 1529 PST.

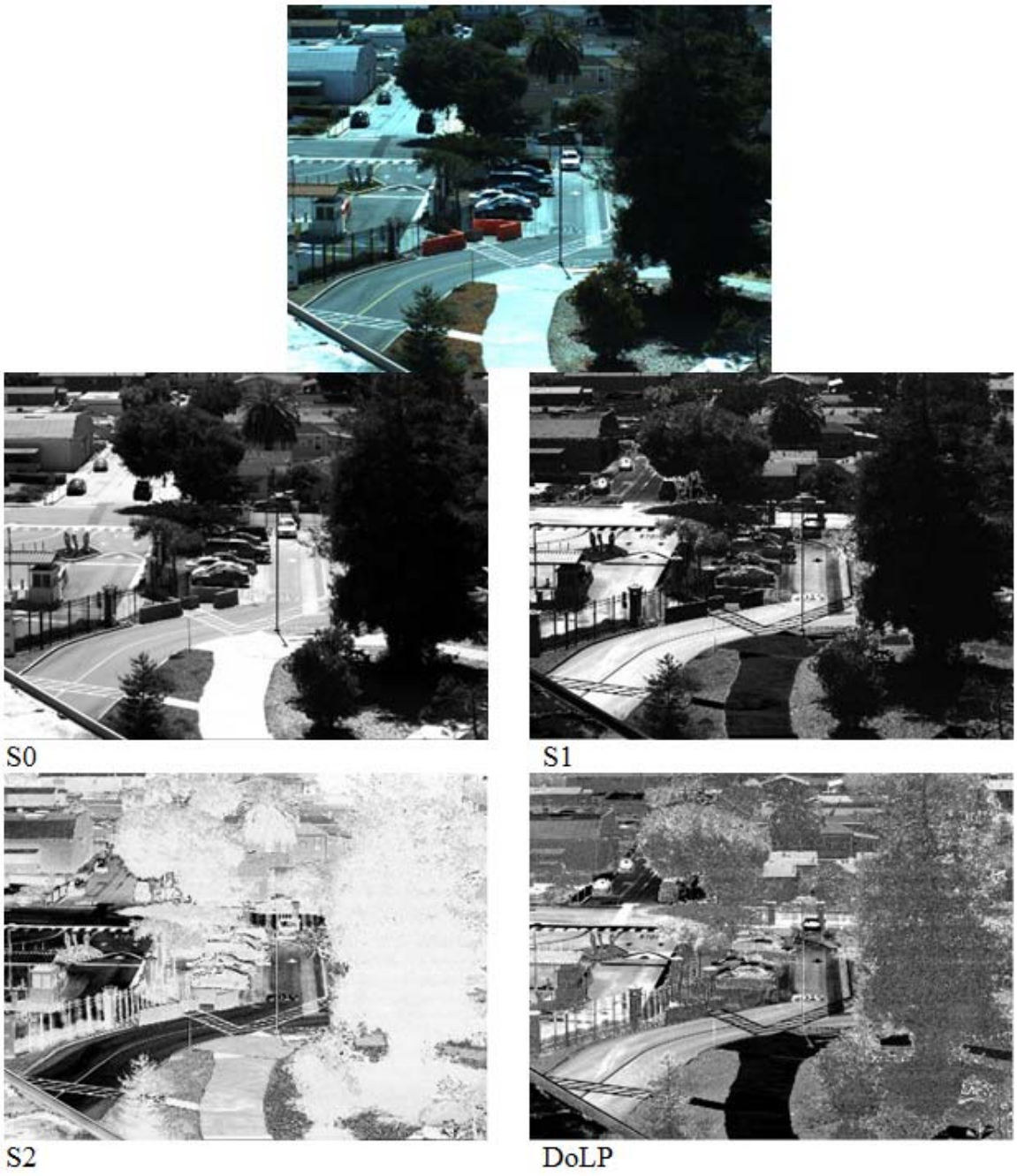

Figure 57. 08 July 2016, 1520 PST.

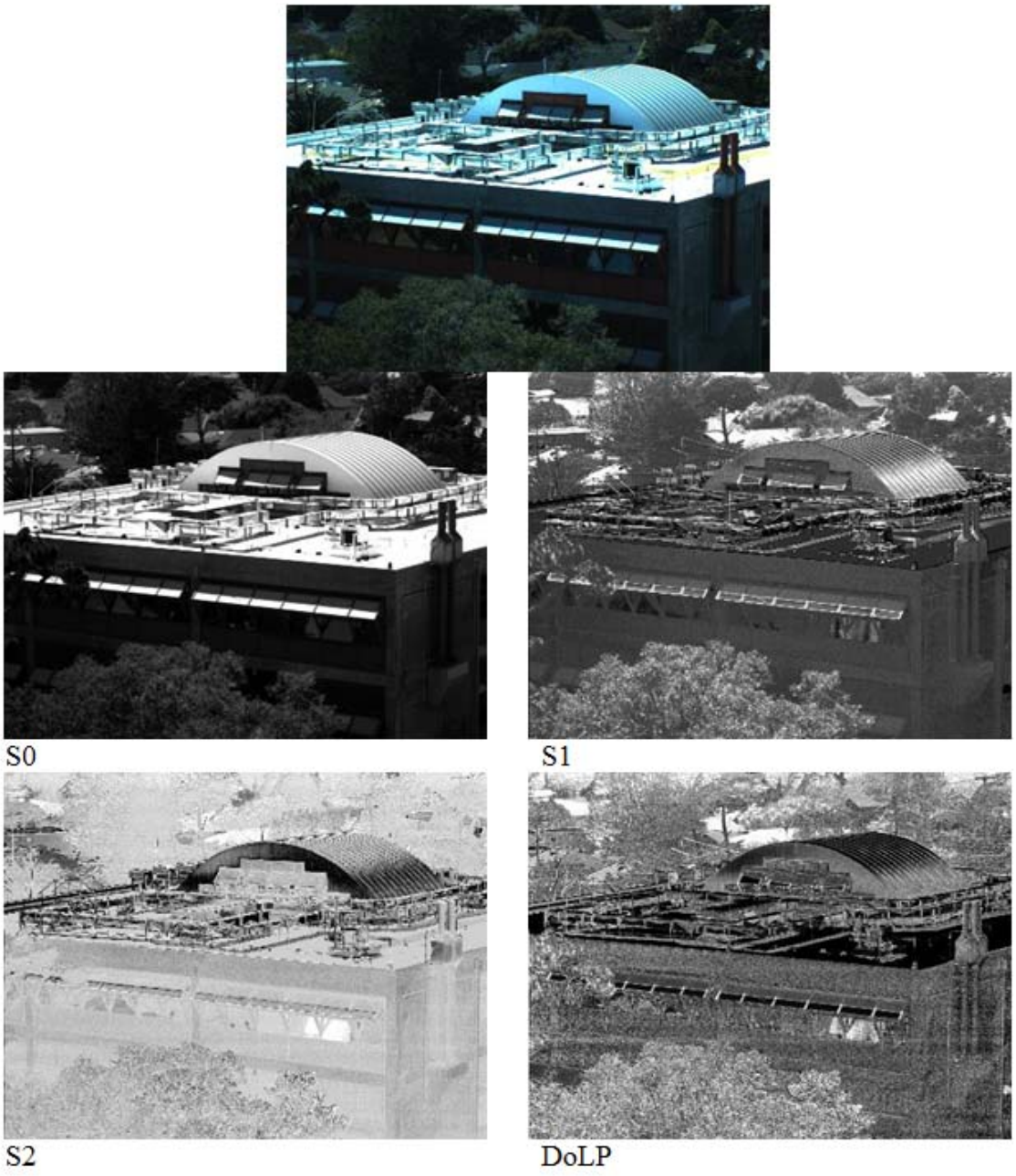

Figure 58. 08 July 2016, 1532 PST.

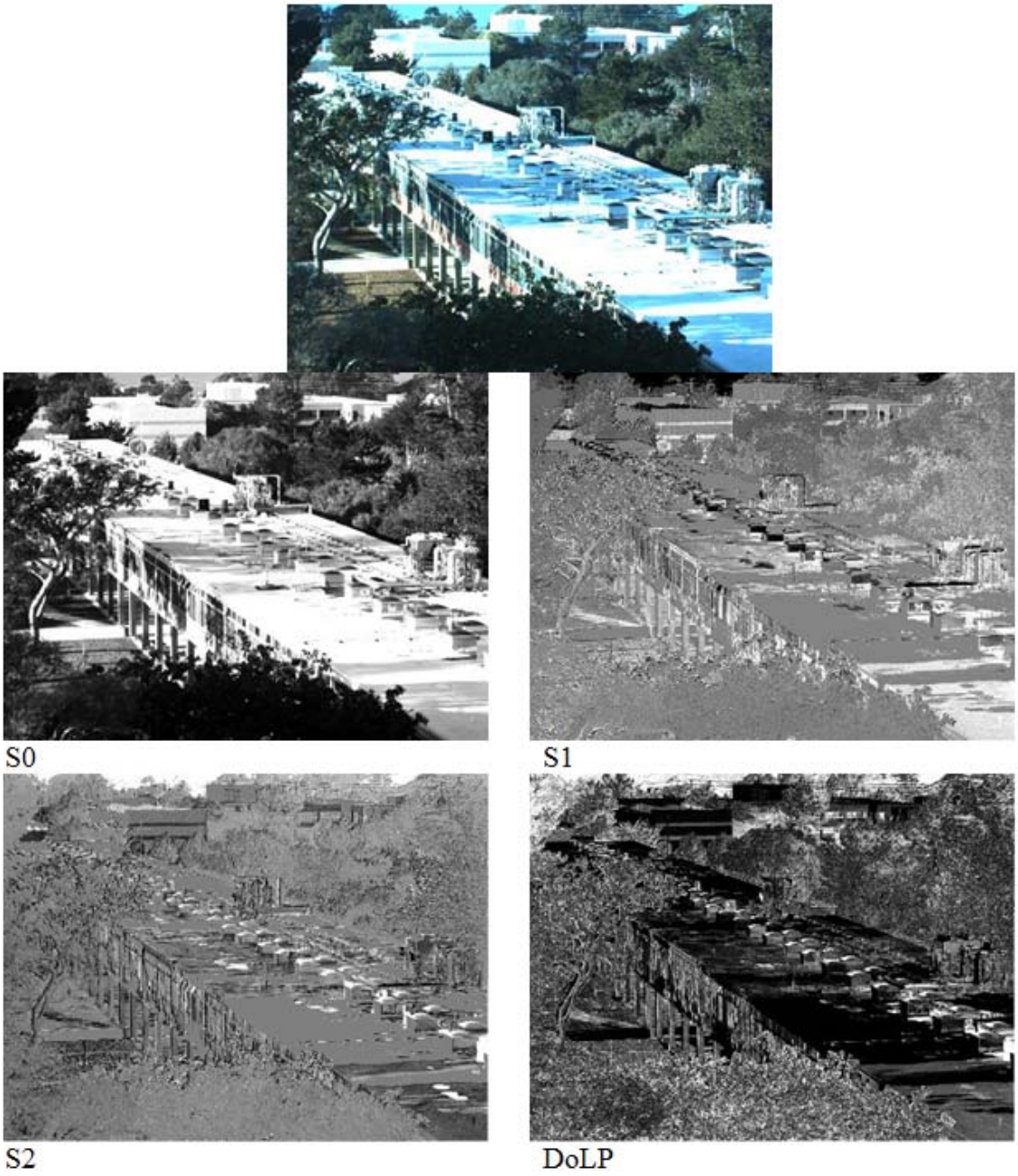

Figure 59. 15 January 2016, 1535 PST.

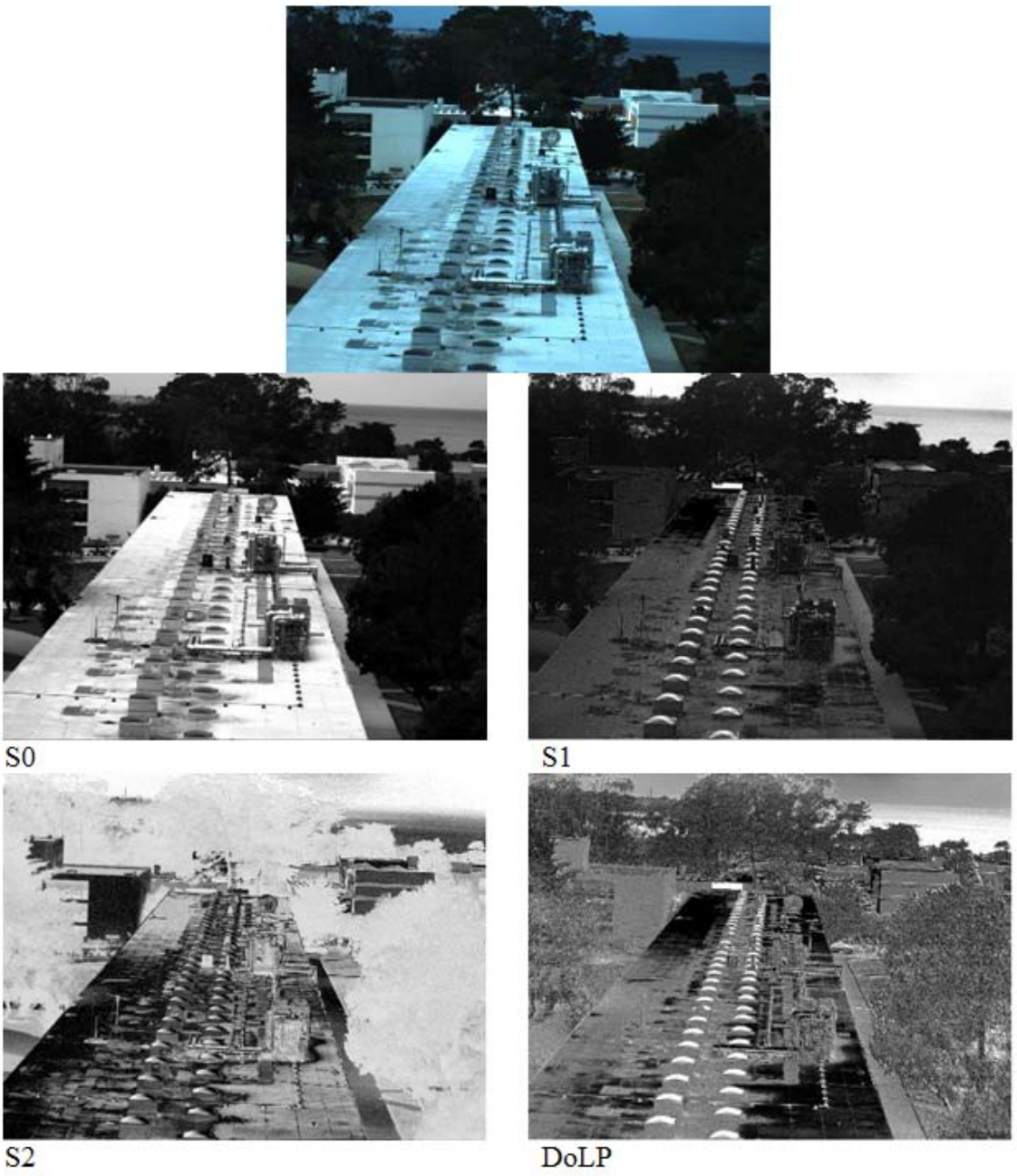

Figure 60. 20 May 2016, 1425 PST.

Figure 61. 20 May 2016, 1442 PST.

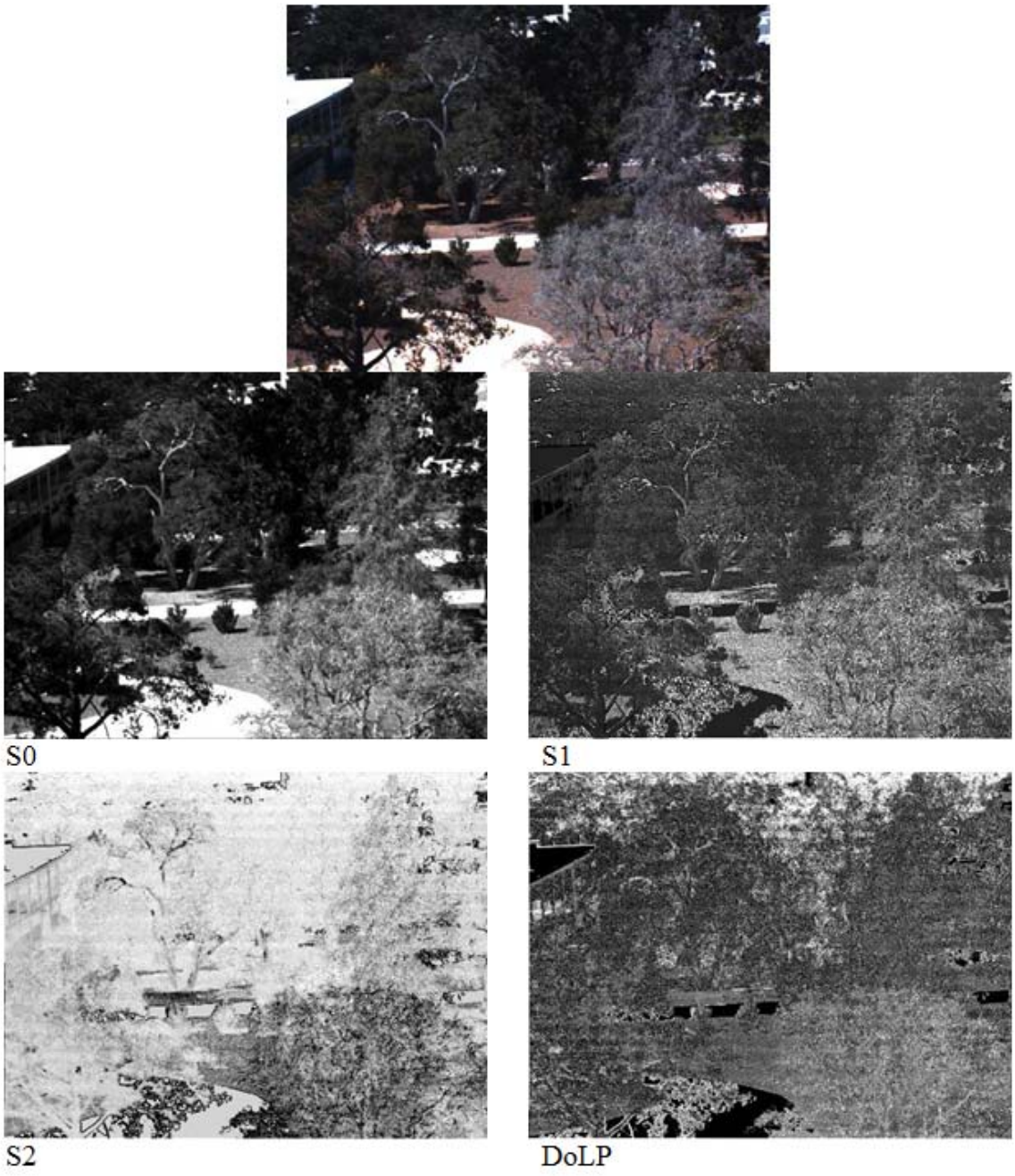

Figure 62. 26 September 2016, 1420 PST.

Figure 63. 29 July 2016, 1540 PST.

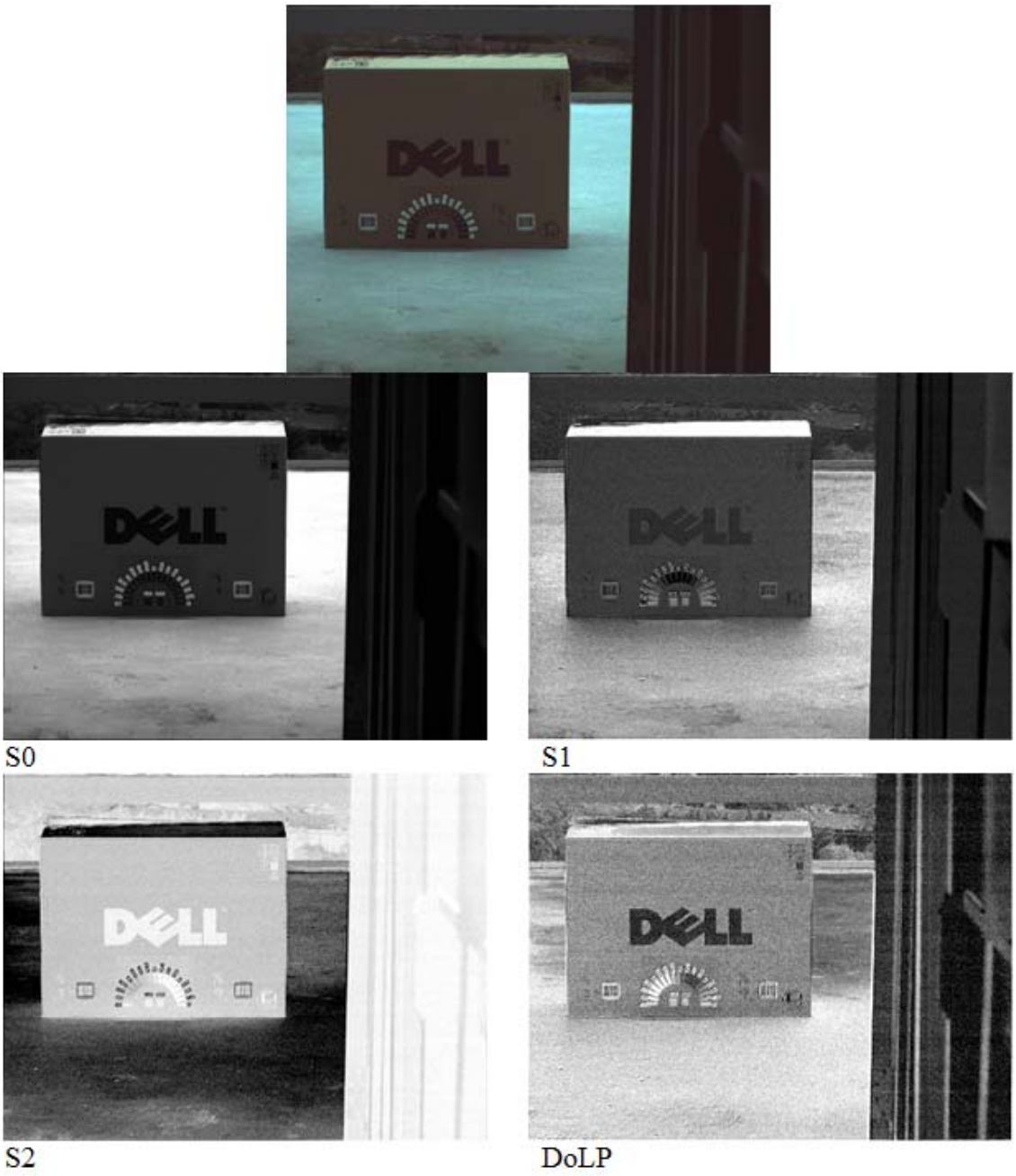

Figure 64. 12 May 2016, 1552 PST.

LIST OF REFERENCES

Azzam, R. M. A., and N. M Bashara. *Ellipsometry and Polarized Light.* Amsterdam: Elsevier, 1977.

Bossa Nova Tech. *Polarization Imaging SALSA Camera Applications*. Venice, CA: Bossa Nova Technologies. Accessed 06 March, 2017. http://www.bossanovatech.com/polarization_imaging.htm.

Boundless.com. "Polarization by Scattering and Reflecting." 2016. Accessed 06 March, 2017. https://www.boundless.com/physics/textbooks/boundless-physics-textbook/wave-optics-26/further-topics-176/polarization-by-scattering-and-reflecting-643-6054/.

Brady, Parrish C. "Scientists Discover New Camouflage Mechanism Fish Use in Open Ocean." Phys.org. November 20, 2015. Accessed 06 March, 2017. https://phys.org/news/2015-11-scientists-camouflage-mechanism-fish-ocean.html.

Brosseau, Christian. *Fundamentals of Polarized Light: A Statistical Optics Approach.* New York: Wiley, 1998.

Chen, H. S., C. R. Nagaraja Rao, Z Sekera, and Air Force Cambridge Research Laboratories (U.S.). *Investigations of the Polarization of Light Reflected By Natural Surfaces*. Los Angeles: University of California, Dept. of Meteorology, 1976.

Collett, Edward, and Society of Photo-optical Instrumentation Engineers. *Field Guide to Polarization* (Bellingham, WA: SPIE, 2005).

Easton, Robert. 2004. "Interaction of Light and Matter." Basic Principles of Imaging Science. Accessed February 13, 2017. https://www.cis.rit.edu/class/simg712-01/notes/basicprinciples-08.pdf.

Eyler, Michael. 2009. "Polarimetric Imaging for the Detection of Disturbed Surfaces." Master's thesis, Naval Postgraduate School, http://calhoun.nps.edu/handle/10945/4719.

Feofilov, P. P. *The Physical Basis of Polarized Emission*. New York: Consultants Bureau, 1961.

Goldstein, Dennis H., and Edward Collett. *Polarized Light*. New York: Marcel Dekker, 2003.

Henderson, Thomas. "Polarization." Light Waves and Color. Accessed February 09, 2017. http://www.physicsclassroom.com/class/light/Lesson-1/Polarization.

Lou, Yunling. *The NASA/JPL Airborne Synthetic Aperture Radar System*. Accessed February 17, 2017. https://airsar.jpl.nasa.gov/documents/genairsar/airsar_paper1.pdf/.

NOAA. "Dual Polarized Radar." NOAA National Severe Storms Laboratory. Accessed February 17, 2017. http://www.nssl.noaa.gov/tools/radar/dualpol/.

Olsen, R. C. 2015. *Remote Sensing from Air and Space.* Bellingham, WA: SPIE—The International Society for Optical Engineering.

Pappas, Stephanie. "How Do We See Color?" LiveScience. April 29, 2010. Accessed February 09, 2017. http://www.livescience.com/32559-why-do-we-see-in-color.html.

Robinson, Philip C. "Polarized Light Microscopy." Nikon's MicroscopyU. Accessed February 09, 2017. https://www.microscopyu.com/techniques/polarized-light/polarized-light-microscopy.

Rowe, M. P., J. S. Tyo, N. Engheta, and E. N. Pugh. "Polarization-Difference Imaging: A Biologically Inspired Technique for Observation Through Scattering Media." *Optics Letters* 20, no. 6 (1995): 608. doi:10.1364/ol.20.000608.

Schott, Brosseau, Christian. *Fundamentals of Polarized Light:* A Statistical Optics Approach. New York: Wiley, 1998.

Shell, James R. *Polarimetric Remote Sensing in the Visible to Near Infrared*. Dissertation, Rochester Institute of Technology. Rochester, NY. http://www.dirsig.org/docs/shell.pdf.

Smith, P. 2008. "The Uses of a Polarimetric Camera." Master's thesis, Naval Postgraduate School, Monterey, http://calhoun.nps.edu/handle/10945/3972.

Smith, Randall B. *Introduction to Interpreting Digital RADAR Images.* January, 4, 2012. Accessed 06 March, 2017. http://www.microimages.com/documentation/Tutorials/radar.pdf.

Swindell, William. *Polarized Light*. Stroudsburg, PA: Dowden, Hutchinson & Ross, 1975.

Temple, Shelby E., Juliette E. McGregor, Camilla Miles, Laura Graham, Josie Miller, Jordan Buck, Nicholas E. Scott-Samuel, and Nicholas W. Roberts. "Perceiving Polarization with the Naked Eye: Characterization of Human Polarization Sensitivity." *Proc. R. Soc. B.* July 22, 2015. Accessed March 06, 2017. http://rspb.royalsocietypublishing.org/content/282/1811/20150338.

Tyo, J. S., E. N. Pugh, and N. Engheta. "Colorimetric Representations for use with Polarization-Difference Imaging of Objects in Scattering Media." *Journal of the Optical Society of America A* 15, no. 2 (February 01, 1998): 367. doi:10.1364/josaa.15.000367.

Tyo, J. S., M. P. Rowe, E. N. Pugh, and N. Engheta. "Target detection in optically scattering media by polarization-difference imaging." *Applied Optics* 35, no. 11 (1996): 1855. doi:10.1364/ao.35.001855.

Tyo, J. Scott, Dennis L. Goldstein, David B. Chenault, and Joseph A. Shaw. "Review of Passive Imaging Polarimetry for Remote Sensing Applications." *Applied Optics* 45, no. 22 (2006): 5453. doi:10.1364/ao.45.005453.

Umansky, M. 2013. "A Prototype Polarimetric Camera for Unmanned Ground Vehicles." Master's thesis, Virginia Polytechnic Institute and State University.

West, D. 2010. "Disturbance Detection in Snow Using Polarimetric Imagery of the Visible Spectrum." Master's thesis, Naval Postgraduate School, Monterey: NPS, http://hdl.handle.net/10945/4963

Zubko, Evgenij, Gorden Videen, Yuriy Shkuratov, Karri Muinonen, and Tetsuo Yamamoto. "The Umov Effect for Single Irregularly Shaped Particles with Sizes Comparable with Wavelength." *Icarus* 212, no. 1 (2011): 403–15. doi:10.1016/j.icarus.2010.12.012.

THIS PAGE INTENTIONALLY LEFT BLANK

INITIAL DISTRIBUTION LIST

1. Defense Technical Information Center
   Ft. Belvoir, Virginia

2. Dudley Knox Library
   Naval Postgraduate School
   Monterey, California